2013-07-30

Health Monitoring and Crack Source Location in Reinforced Concrete Based on Acoustic Emission

Tala Shokri
University of Miami, t.shokri@umiami.edu

UNIVERSITY OF MIAMI

HEALTH MONITORING AND CRACK SOURCE LOCATION IN REINFORCED CONCRETE BASED ON ACOUSTIC EMISSION

By

Tala Shokri

A DISSERTATION

Submitted to the Faculty
of the University of Miami
in partial fulfillment of the requirements for
the degree of Doctor of Philosophy

Coral Gables, Florida

August 2013

UNIVERSITY OF MIAMI

A dissertation submitted in partial fulfillment of
the requirements for the degree of
Doctor of Philosophy

HEALTH MONITORING AND CRACK SOURCE LOCATION IN REINFORCED CONCRETE BASED ON ACOUSTIC EMISSION

Tala Shokri

Approved:

Antonio Nanni, Ph.D. Professor and Chair of Civil, Architectural & Environmental Engineering	M. Brian Blake, Ph.D. Dean of the Graduate School
Ronald Zollo, Ph.D. Professor of Civil, Architectural & Environmental Engineering	Paul Ziehl, Ph.D. Professor of Civil & Environmental Engineering University of South Carolina
Carol Hays, Ph.D. Professor in Practice of Civil, Architectural & Environmental Engineering	

SHOKRI, TALA (Ph.D., Civil Engineering)
(August 2013)

Health Monitoring and Crack Source Location in Reinforced Concrete Based on Acoustic Emission

Abstract of a dissertation at the University of Miami.

Dissertation supervised by Professor Antonio Nanni.
No. of pages in text. (99)

The process of implementing a damage identification strategy for infrastructure is referred to as Structural Health Monitoring (SHM). This term has been used in the last decades to describe a range of systems implemented on constructed facilities, including Reinforced Concrete (RC), for the purpose of informing owners/operators on the condition of structures that experience gradual or sudden changes to their state of serviceability. The increased interest in SHM and its associated potential is due to its significant life-safety and economic benefits. Within the family of non-destructive test methods, Acoustic Emission (AE) is classified as a passive technology capable of providing information useful in locating active cracks in structural members. AE crack locating methods are affected by signal attenuation and dispersion of elastic waves due to macro inhomogeneity and the geometry of RC structural members. AE methods of crack location are already well established in steel structures but due to the heterogeneous nature of concrete accuracy, identification, and the attenuation of acoustic waves are still areas where development is needed. The goal of this dissertation is to advance AE technology applied to RC structures in order to locate cracks and to study wave propagation in relation to variables common to concrete mixture design and structural

element geometry. The investigation is divided into three studies. The first study, considers the sources of uncertainty in the AE crack location process. A methodology is proposed to capture and locate events that are associated with cracks in RC members during loading and unloading regimes. In particular, the relationship between crack events and load is analyzed to assess the feasibility of using AE information to evaluate the cracking behavior of two RC slab strips as load is applied.

A second study experimentally and analytically investigates the relationship between AE wave attenuation and velocity and the variables of RC constituent materials and structural geometry. To this end, ten slabs with variable parameters including strength, unit weight, aggregate size, aggregate type, geometry and presence of steel reinforcement were cast. AE signals were generated at known locations on the slab surface using Pencil Lead Breaks (PLBs), an ASTM standard method, and recorded by four AE sensors. Results confirm the effects of the above-named parameters on attenuation and velocity of acoustic waves. The outcomes of this study can be used to develop a reference database for AE wave attenuation and velocity applicable in the field for SHM of concrete members.

The last study experimentally investigates the effects of cracks on AE wave propagation (attenuation and velocity). Two similar RC slabs are manufactured and load tested. In parallel with the well-established measurements of load and strain, an active AE monitoring is carried out throughout the load test. Variable AE wave velocity is introduced, tabulated and correlated to crack depth ratio as parameter describing the severity of crack in the RC member. The results show that cracks can prominently affect the attenuation and velocity of AE waves.

To my fiancé Navid,
and my parents Pari and Mahmood
with love and gratitude

ACKNOWLEDGEMENTS

This work was performed with the support of the U.S. Department of Commerce, National Institute of Standards and Technology, Technology Innovation Program, Cooperative Agreement Number 70NANB9H9007. I would like to thank them for their support and I hope my research has been worthy of their investment.

TABLE OF CONTENTS

LIST OF TABLES

LIST OF FIGURES

CHAPTER 1: INTRODUCTION

The process of implementing a damage identification strategy for infrastructure is referred to as Structural Health Monitoring (SHM). This term has been used in the last decades to describe a range of systems implemented on constructed facilities (including Reinforced Concrete (RC)) with the purpose of assisting and informing owners/operators on the condition of structures under gradual or sudden changes to their state of serviceability. At the simplest level and with reference to RC, recurrent visual observation and assessment of structural condition (e.g., corrosion, cracking, spalling and deformations) could be viewed as SHM activities. A wide variety of highly effective local non-destructive evaluation tools are available for such monitoring. The increased interest in SHM and its associated potential is due to its significant life-safety and economic benefits. For long-term SHM, the output of this process is periodically updated information regarding the ability of the structure to continue to perform its intended function in light of the inevitable aging and degradation resulting from the operational environments.

The Acoustic Emission (AE) technique plays a progressively significant role in the field of Non-Destructive Techniques (NDT) especially in SHM. AE monitoring is arguably based on the simplest physical concepts (nearly everyone has heard audible AE in the form of popping and cracking noises from materials under stress), but is one of the most difficult NDT methods to practically implement. A formal definition of the AE phenomenon is often given as the release of transient elastic waves in solids as a result of rapid localized redistributions of stresses which accompany the occurrence of damage

mechanisms. Examples of AE events related to civil engineering materials include crack growth in steel and concrete, corrosion for metals, fiber breakage, and matrix debonding for composites.

Within the family of NDT methods, AE is classified as a passive technique providing capability to detect and locate damage in structural members. AE location methods are already well established in composite and steel structures (Gong et al. 1992 and Gostautas et al. 2005), but due to the inhomogeneous nature of concrete their successful use for SHM of concrete members still faces several challenges and there are areas where development is desirable (Grosse and Ohtsu 2008 and Muhamad Bunnori et al. 2006). AE monitoring is affected by the signal attenuation and dispersion of elastic waves due to material inhomogeneity and member boundaries. Reinforced concrete (RC), being a composite of cement paste, fine and coarse aggregate and steel reinforcement, cannot be assumed to be non-dispersive as any homogeneous and isotropic material and this affects the wave propagation (Miller and McIntire, 1987 and Muhamad Bunnori et al. 2006). Having a poor understanding of AE wave propagation in RC members can lead to lack of full coverage in a member being monitored and makes AE source location technique incorrect and in many cases impossible. In recent years, there has been considerable research work regarding wave propagation in concrete members using other nondestructive techniques (Gassman and Tawheed 2004, Philippidis and Anggelis 2005, Kim et al. 2006 and Chang et. al. 2006), but studies investigating the relationship between AE wave propagation and properties of concrete have been lacking.

This thesis consists of three studies that cover AE source location, attenuation and velocity in concrete members. In the first study an attempt has been made to relate the

results obtained during a load test performed on two RC slab strips to the corresponding AE data in order to evaluate the application of the AE technique for determination of crack location and propagation in a concrete member. Two identical strips of a one-way RC slab of the first floor of the building are saw cut and loaded to failure. The AE signals reflecting the release of energy taking place during the damage process are recorded and by analyzing these recorded signals, cracks are located. AE wave attenuation and velocity are assessed to be of paramount importance of AE application and if incorrectly are assumed, can make the AE source location impossible or inaccurate. In this study, sources of uncertainty in the crack location approach are considered and a novel methodology to improve the accuracy of crack location results is presented. It is obtained that to have an accurate AE crack source location a pre-test is needed to evaluate the given member. In order to avoid the pre-test and make the AE location procedure less time consuming and costly in the field, an attempt is made in the second study to establish a database for AE wave attenuation and velocity in variable RC members.

The aim of the second study is to experimentally characterize the role of concrete constituents and geometry on AE wave propagation. Accordingly, slabs with variable parameters including strength, unit weight, aggregate size, aggregate type, geometry and presence of steel reinforcement are cast to allow exploring attenuation and velocity of AE waves. A procedure to calculate AE wave velocity in un-cracked concrete is introduced and the effect of waveform analysis on velocity determination is investigated. Results obtained from this study are utilized to provide information on wave attenuation and velocity in concrete in form of two reference tables which can be applicable for AE in-situ tests.

Based on the outcome of the first study, the other factor that makes AE source location technique less effective is cracking. For AE to be a practical method to locate and assess damages and cracks in RC members, a clear and practical understanding of the velocity and attenuation of the acoustic wave in both cracked and un-cracked situation is essential. In the third study an attempt has been made in order to understand the changes in characteristics of AE waves while passing through a cracked RC slab. To do this, two RC slabs are manufactured loaded in a four point bending setup. The loading pattern is designed to take into account loading and unloading stages in order to investigate both open and closed crack situations. Effects of cracking parameters including maximum crack depth, maximum crack width and number of cracks are discussed and crack to slab depth ratio is chosen for correlation with AE wave velocity and attenuation. The Results obtained from this study are utilized to provide information on wave attenuation and velocity in cracked RC slabs in form of two tables that can be used as part of a reference database that can be applicable for AE in-situ tests and SHM purposes. The results from the third study complement the database for un-cracked concrete slabs proposed in the second study.

CHAPTER 2: STUDY 1 – CRACK SOURCE LOCATION BY ACOUSTIC EMISSION MONITORING METHOD IN RC STRIPS DURING IN-SITU LOAD TEST

SUMMARY

Various monitoring techniques are now available for structural health monitoring and Acoustic Emission (AE) is one of them. One of the major advantages of the AE technique is its capability to locate active cracks in structural members. AE crack locating approaches are affected by the signal attenuation and dispersion of elastic waves due to inhomogeneity and geometry of reinforced concrete (RC) members. In this paper, a novel technique is described based on signal processing and sensor arrangement to process multisensory AE data generated by the onset and propagation of cracks and is validated with experimental results from an in-situ load test. Considering the sources of uncertainty in the AE crack location process, a methodology is proposed to capture and locate events generated by cracks. In particular, the relationship between AE events and load is analyzed, and the feasibility of using the AE technique to evaluate the cracking behavior of two RC slab strips during loading to failure is studied.

BACKGROUND

This study is an attempt to relate the results obtained during a load test performed on two RC slab strips to the corresponding AE data in order to evaluate the application of the AE technique for determination of crack location and propagation in a concrete member. The experiments are performed in a three-story apartment building built in 1947 and scheduled for demolition. Two identical strips of a one-way RC slab of the first floor of the building are saw cut and loaded to failure. The AE signals reflecting the release of

energy taking place during the damage process are recorded and by analyzing these recorded signals, cracks are located. In this paper, sources of uncertainty in the crack location approach are considered and a novel methodology to improve the accuracy of crack location results is presented. In this method, a sensor placement technique considering the signal attenuation and failure mechanism of the strips is introduced. The study introduces a method to detect the onset and propagation of cracks and their location in a RC member using AE signals. For this method to be employable, a framework for data preparation and analysis including sensor arrangement, wave velocity optimization and data filtering is proposed.

2.1 CRACK LOCATION METHOD

AE is a phenomenon of transient stress waves resulting from a sudden release of elastic energy caused by mechanical deformations, initiation and propagation of microcracks, dislocation movement and other irreversible changes in material (ASTM E1316 2010). Sensors placed on the surface of structural members may be utilized to detect the acoustic waves produced by a source. A signal that exceeds a defined threshold is called “hit” and triggers the accumulation of data. If the same signal is recorded by more than one sensor, it is considered to be illustrative of a significant incident and called “event”. If sufficient information about an individual event is obtained, the location of the AE source can be determined (Carpinteri et al. 2008).

The basis for the location calculation is the simple time-distance relationship implied by the velocity of the sound wave which is called point location. The absolute arrival time, t, of a hit in an event can be combined with the velocity of the sound wave, v, to yield the distance, d, from the sensor to the source:

$$d = vt \tag{1-1}$$

In this formula, the velocity is constant and the distance d_i between the source of unknown coordinates (x_0, y_0, z_0) and sensor i with known coordinates (x_i, y_i, z_i) can be found as (Miller and Mclntire 1987):

$$d_i = \sqrt{(x_i - x_0)^2 + (y_i - y_0)^2 + (z_i - z_0)^2} \tag{2-2}$$

The distance of the source to the sensor "i" can also be given by:

$$d_i = v(t_i - t_0) \tag{2-3}$$

Where t_i is the arrival time to sensor i and t_0 is the time of event occurrence.

This calculation is complicated by the lack of knowledge of the exact time the event originated. To get around this problem, all the times are considered relative to the first hit in the event. Each arrival time difference implies a difference in distance to the sensor relative to the distance to the first hit sensor (Shull 2002 and Salinas et al. 2010). For the second sensor, $i=2$, relative to the first sensor, $i=1$, a difference equation can be written as:

$$t_2 - t_1 = (d_2 - d_1)/v \tag{2-4}$$

Considering a two-dimensional (plane) geometry, where x_0 *and* y_0 are the unknown coordinates of the source, Eq. (2-2) can be combined with Eq. (2-4) to yield:

$$t_2 - t_1 = \left[\sqrt{(x_2 - x_0)^2 + (y_2 - y_0)^2} - \sqrt{(x_1 - x_0)^2 + (y_1 - y_0)^2}\right]/v \tag{2-5}$$

This equation contains two unknowns (x_0 and y_0) and cannot be solved by itself. To get a second equation with the same two unknowns, a third sensor should be added producing equation:

$$t_3 - t_1 = \left[\sqrt{(x_3 - x_0)^2 + (y_3 - y_0)^2} - \sqrt{(x_1 - x_0)^2 + (y_1 - y_0)^2}\right]/v \qquad (2\text{-}6)$$

These simultaneous equations can then be solved for x_0 *and* y_0. The math becomes more complicated when extended to three dimensions (volumetric), but the approach remains the same (AEwin Software User's Manual 2009).

The accuracy of AE location method in RC members is affected by several factors, including the heterogeneous nature of the material system. Even if a crack is located, the error can be large depending on the size of the tested structure and the distance of the sources to the sensors (Grosse and Ohtsu 2008). Moreover, in practical applications, crack location must be obtained from the useable portion of very large data set. The sources of crack location error are listed as follow.

Attenuation: Attenuation dampens a stress wave as the wave front propagates away from its origin and spreads over a larger volume. Attenuation of a body stress wave in an infinite medium causes the wave amplitude to decrease proportional to the distance from the wave source (Miller and Mclntire 1987). RC has unique characteristics due to heterogeneity, porosity and presence of steel reinforcement. Cracks dampen the progressing wave or, when wide enough, can become barriers to wave transmission. Besides internal damping, AE waves travelling in RC members can undergo reflection, scattering, mode conversion and diffraction, where all this influences the propagation of stress waves (Miller and Mclntire 1987). Therefore, attenuation is considered as having the major influence on the accuracy of data collected from RC members and should be determined prior to a test.

Sensor Number and Configuration: For a point source to be identified, signals must be detected by a minimum number of sensors: two for linear, three for planar, four for

volumetric media. However, using more sensors than necessary, improves accuracy (Miller and Mclntire 1987). Also, source location accuracy is strongly affected by the relative position of sensors in a sensor array (Guratzsch and Mahadevan 2010). In general, the location accuracy is best in the area enclosed by the sensors and decreases as sources move outside this area (Tobias 1976 and Miller and Mclntire 1987).

Velocity: Accurate knowledge of wave velocity is critical for source location (Muhamad Bunnori et al. 2006) and, prior to any test, it has to be attained. For RC members in particular, wave velocity may not remain constant during the performance of a test as cracks develop as a function of the applied load.

Time of Arrival (TOA): Because of the presence of surfaces, several modes of wave propagation exist within a body. Compression (P) waves mostly are used to investigate the location of a source in three-dimensional (3D) media (Muhamad Bunnori et al. 2006 and Grosse and Finck 2006). In this case, the major error in source location is due to the miscalculated TOA of an AE hit. Estimating the correct TOA for the P wave is a challenge especially when a wave propagates through concrete. Literature shows that interpretation of AE data by an expert manually processing the data and selecting the signal TOA can improve location accuracy significantly (Miller and Mclntire 1987). Although for large data set, this is not possible and automation is indispensable. The automatic determination of TOA can be based on a threshold (in dB scale) which is specific to a particular material and transducer. TOA is calculated from the first signal excursion above the threshold. Therefore, the choice of the threshold value is crucial to the quality of the TOA selection and location results (Miller and Mclntire 1987).

Frequency Band: To lessen the effect of noise present in an AE signal, an appropriate frequency filter setting should be selected. Frequency filters are used to reduce low-frequency mechanical noise and high-frequency electronic noise. The correct choice of frequency band has a critical effect on the detection range of the sensor and the vulnerability of the setup to background noise.

2.2 METHODOLOGY OF AE MONITORING OF CRACKS

In this study, the point location technique based on the differences in TOAs of the signals generated from the cracks and recorded by a number of sensors is used for crack location. However, recognizing the challenges of AE monitoring in RC members with the objective of crack location especially in a situation where thousands of events may be recorded, a simple location algorithm is not sufficient (Miller and Mclntire 1987). Consequently, to improve the precision of the crack location obtained with the equipment and methodology used, a procedure is suggested that consists in performing an AE pre-test aimed at establishing the following: attenuation curves and sensor arrangement (including sensor spacing, number and configuration), threshold, velocity, and frequency band selection.

2.3 EXPERIMENTAL OBSERVATION AND RESULT

2.3.1 Geometries, Material and Instrumentation

The structure of interest consisted of a RC frame and infill masonry walls. To investigate the one-way RC slab behavior, two 30-inch (762-mm) wide strips were cut through one of the slabs of the building and load tested (**Fig. 2-1**).The relevant geometry and material properties of the RC slab are given in **Table 2-1.** The width of the strips is selected so

that three reinforcing bars are included in the cross-section. The centerlines of the two slab strips are 5 ft (1.52 m) apart. For both slab strips, the test load is applied at two points placed at one-third of the total span. The load test is conducted using a push-down loading configuration. **Fig. 2-2** shows a picture of the load test setup.

2.3.2 AE Equipment

In this research, the PAC Sensor Highway II system (AEwin Software User's Manual 2009) equipped with R6I-AST resonance sensors is used for AE data collection. This system with 16 high-speed AE channels is designed for unattended and remote monitoring use, and includes AEWin software (AEwin Software User's Manual 2009) for data analysis. The R6I-AST resonance sensors have an operating frequency range of 40 - 100 kHz and a resonant frequency of 55 kHz. The "I" designation indicates that the sensor has a built-in 40 dB preamplifier. To ensure proper coupling of each AE sensor, a two-part epoxy contact agent is applied to connect the sensors to the concrete surface.

2.3.3 AE Pre-test

Setup and Measurements. The AE pre-test is performed on the slab in its original condition (pre-cut) by Pencil Lead Breaks (PLBs) at given locations to generate acoustic waves while the sensors are recording. PLB is an ASTM standard method to produce similar AE events (ASTM E 976 2010). The arrangement of the sensor for the AE pre-test (different from the one for the load test) is given in **Fig. 2-3,** which shows the location of five sensors with respect to the slab perimeter walls. Four sensors are placed in a rectangular fashion for the attenuation and wave propagation to be investigated in three directions. The fifth sensor is mounted at the center of this rectangle for location

error considerations given that the proper arrangement of sensors requires equilateral triangle geometry (Vannoy et al. 1991). Using the standard 0.5 mm (0.019 in) diameter lead, PLBs are conducted at 3 in (76.2 mm) intervals between the sensors along the lines S_1-S_2; S_1-S_3; and, S_1-S_4. In order to minimize and uniformly distribute the operator errors, the PLBs are repeated three times at each position following a fully randomized order. The data is collected and analyzed before the load test.

Data processing and results. **Fig. 2-4** shows the flow chart of the method of analysis for the AE pre-test that intends to reduce the location error. The following describes each column in the flow chart in more details together with experimental results.

Column 1

This column consists of these steps:

a) Deriving attenuation curves for different directions

b) Obtaining the level of environmental noise amplitude

c) Deriving the attenuation limit

d) Finding the effective radius of efficacy (Res) of a sensor

In step (a) of column 1, six attenuation curves shown in **Fig. 2-5** are derived for three PLB paths of **Fig. 2-3**. For each line between sensors (three directions) two curves are obtained. Attenuation limits maximum sensor distance, which, consequently, limits the area that can be accurately monitored by a fixed number of sensors.

In step (b), the level of the environmental noise amplitude is measured by acquiring AE data for four hours after the PLB test and a maximum noise level of 60 dB is determined.

In step (c), the objective is to find "attenuation limit" above which recorded signals due to crack propagation would not be recognizable from the environmental noise. The maximum detectable amplitude for R6I sensors is 100 dB, corresponding to the amplitude of the amplified signal when it reaches 10 volts (saturation limit of the system). However, the goal is set for concrete cracks with source amplitudes over 90 dB to be detected. As a result, 30 dB (i.e., 90-60) is selected as the "attenuation limit" (**Fig. 2-5)**.

In step (d), in order to optimize the positioning of the sensors, a case-dependent parameter termed Radius of Efficacy of Sensor (R_{es}) is introduced. R_{es} is defined as the distance from a sensor within which no source of AE can be overshadowed by noise. This parameter plays a major role in arranging the sensors and is calculated from the attenuation curves considering the attenuation limit.

Since the R_{es} is a scalar value to be effective in all directions, it is chosen from the path with the largest attenuation corresponding to the path S_1-S_4 (**Fig. 2-5 c**) in this case. Accordingly, the distance of 35 in (0.89 m) corresponding to the attenuation limit of 30 dB, is set as the R_{es}. Therefore, the sensor arrangement for the load test should be designed in a way that at least four sensors enclose the area of expected damage using R_{es} 35 in (0.89 m).

Column 2

Column 2 displays the procedure to find the proper post processing threshold to be applied for TOA selection of AE load test data. This column consists of these steps:

a) Selecting the arrival times of PLBs manually

b) Recording the corresponding thresholds for all arrival times

c) Calculating the average of all recorded thresholds

In step (a) of column 2, waveforms recorded from PLBs performed between the sensors (**Fig. 2-3**) are used for TOA selection. For each line (S1-S2, S1-S3, S1-S4), the arrival times of the PLBs located on that line to the end sensors are selected manually based on their waveforms.

In step (b), the corresponding threshold for each TOA is recorded.

In step (c), the average of all recorded thresholds, 34 dB, is chosen to be imposed to AE load test data in post processing step.

Column 3

Column 3 demonstrates the procedure to calculate the optimal wave velocity through the RC member under consideration. This column consists of these steps:

a) Selecting the arrival times manually

b) Defining the overall error based on calculated and known locations of the PLBs

c) Minimizing the overall error

d) Finding the optimal velocity

In step (a) of column 3, the manually picked arrival times, described in column 2 step a, are collected for velocity calculation.

In step (b) and (c) of column 3, the optimal velocity is defined so that the overall error, E_D, between the difference of calculated distances $\Delta d_j = (d_2 - d_1)_j$ of PLB j to the end sensors and their actual values, $\Delta D_j = (D_2 - D_1)_j$, is minimized. For each break located between the sensors along the lines S_1-S_2, S_1-S_3, and S_1-S_4 (**Fig. 2-3**), d_2 and d_1 are the

calculated distances of PLB j to the end sensors and D_2 and D_1 are the exact distances. Defining the error as:

$$E_D^2 = \sum_{j=1}^{n}\left(\Delta D_j - \Delta d_j\right)^2 = \sum_{j=1}^{n}\left(\Delta D_j - v\Delta \mathrm{t}_j\right)^2 \quad (2\text{-}7)$$

Where $\Delta t_j = (t_2 - t_1)_j$ and manually picked arrival times of PLB j to the end sensors can be used as t_1 and t_2 .This can be minimized by:

$$\frac{\partial E_D^2}{\partial v} = 0 \rightarrow \sum_{j=1}^{n} \Delta \mathrm{t}_j\left(\Delta D_j - v\Delta \mathrm{t}_j\right) = 0 \quad (2\text{-}8)$$

Resulting in the optimal velocity, v of:

$$v = \frac{\sum_{j=1}^{n} \Delta \mathrm{t}_j \Delta D_j}{\sum_{j=1}^{n} \Delta {\mathrm{t}_j}^2} \quad (2\text{-}9)$$

In step (d), by substituting all arrival times selected in step (a) and known location of PLBs in Eq. (2-9) the optimal velocity is calculated. As a result, the optimal velocity of 120,000 in/s (3048 m/s) is used for AE source location during the load test.

Column 4

To find the frequency band, an iterative procedure is developed. In this iterative procedure the low-frequency end is constant and the high-frequency end is changing. This procedure consists of these steps:

a) Uploading the PLBs data into AEWin software and setting the initial frequency band
b) Frequency filtering of PLBs waveforms
c) Calculating PLBs locations using filtered waveforms
d) Adding 10 kHz to the upper frequency end (up to 300 kHz)

e) Repeating steps (b) and (c)

f) Exporting all calculated locations of PLBs into a database

g) Calculating the square root of the sum of the squares (SRSS) error

h) Finding the minimum of SRSS errors

i) Finding the best frequency band

In step (a) of this procedure, the AE pre-test AE data including PLB waveforms is uploaded into AEWin software. Since sensor manufacturer recommends low-frequency end of 20 kHz in highly attenuating material (AEwin Software User's Manual 2009), the Low-frequency end is constant at 20 kHz .The initial high-frequency end is set at 100 kHz.

In step (b), using the frequency band, all the waveforms are filtered.

In step (c), AEwin point location build-in algorithm (AEwin Software User's Manual 2009) is operated to find the location of all PLBs. Referring to point location technique and Eq. (2-5) and (2-6), for this algorithm to be applicable, the differences in TOAs of signals recorded by sensors, wave velocity and known location of sensors are needed. To attain that, the TOAs extracted from PLBs filtered waveforms recorded by all five sensors, known location of five sensors (**Fig. 2-3)** and the optimal velocity of 120,000 in/s (3048 m/s) are imposed to the location algorithm. The procedure in steps (b) and (c) iterates and in each iteration10 kHz (up to 300 kHz) is added to previous upper frequency end and new locations for PLBs are calculated.

In step (d), the calculated locations of PLBs, from all iteration, are exported to a Matlab program for error analysis.

In steps (e) and (f), the objective is to find the best frequency band based on the minimum error between exact and calculated location of PLBs. The collective (overall) error is defined as the SRSS of the distances of all PLBs (exact position) from their respective calculated location, or in mathematical terms:

$$E_{XY}^2 = \sum_{j=1}^{n} \left[\left(X_j - x_{cj} \right)^2 + \left(Y_j - y_{cj} \right)^2 \right] \quad (2\text{-}10)$$

Where E_{XY} denotes the error, (X_j, Y_j) the exact coordinates of the PLB j, (x_{cj}, y_{cj}) the computed coordinates and n the number of PLBs. This program calculates the collective error for each repetition (frequency band). In step (g), the high-frequency end corresponding to the best result (minimum collective error), 150 kHz, is chosen as the selected high-frequency end. Therefore, 20-150 kHz frequency band is selected for the AE data analysis during the load test.

The AE pre-test necessary for all field applications produces the following parameters:

- Res (i.e., 35 in (0.89 m))
- Threshold (i.e., 34 dB)
- Velocity (i.e., 120,000 in/s (3048 m/s))
- Frequency band (i.e., 20-150 kHz)

2.3.4 Load Test

Loading procedure. The load test is conducted according to the cyclic loading protocol described in ACI 437 (ACI 437R-03 2003). After conducting the cyclic load test, the slab strips are loaded to failure. This study only covers on the load testing to failure. The experimental and theoretical results of the cyclic load test are discussed by De Luca et al (2011).

AE Monitoring. Due to the limited number of sensors that could be attached to the instrument (16 sensors in total) only eight sensors are used for each slab strip. The optimal position of the sensors is designed using AE pre-test data analysis. Since the test is carried out to ultimate failure, the area of interest is the mid span of the strips. Four sensors are assigned to the area between the load points. Recognizing that the R_{es} of each sensor is 35 in (0.89 m), as many as four sensor could cover zone of concern where crack formation is predicted (**Fig. 2-6**). To reduce noise, two sensors at each end of the strips are used as guard sensors (i.e., sensors S_1, S_2, S_7 and S_8 (**Fig. 2-6**)). This is a noise rejection technique based on wave arrival times: if an AE wave is detected first by a guard sensor, it is ignored in the analysis as it is assumed that the source of the wave is outside the area of interest.

Crack location procedure. **Fig. 2-7** presents the crack location procedure based on the outcome of the AE pre-test. This procedure consists of these steps:

a) AE recording
b) Extracting noise using guard sensors
c) Frequency filtering
d) Applying calculated threshold for TOA selection
e) Employing the wave velocity to the location algorithm
f) Locating the cracks

In step (a), the AE recording begins along with the load testing to failure and AE data is acquired continuously. In step (b), after conducting the load test, noise is extracted from the AE data using the guard sensors. In step (c), the data is filtered using frequency band of 20 kHz - 150 kHz.

In step (d), the TOAs of all hits are selected by applying calculated threshold of 34 dB on the filtered data. In step (e), the optimal velocity of 120,000 in/s (3048 m/s) is imposed to the AEwin point location built-in location algorithm.

At the end, in step (f), by knowing the exact location of the sensors, the wave velocity of signal through material and the time differences between the hits (Eq. (2-5) and (2-6)), the events (cracks) are determined and AEwin point location built-in algorithm is operated to map the crack location. The two strips have almost identical behavior, thus only the results from strip 2 are presented here.

2.4 RESULTS AND DISCUSSION

By applying the procedure described in **Fig. 2-7**, events generated from the cracks are captured and located after they occurred in midspan of strip. This allows for the monitoring of crack formation and comparison with visible cracks on the surface during the load test.

In a sequence, the recorded AE events at the midspan during three load segments from 0-9000 lb (40.0 kN) are shown in **Fig. 2-8.** Theoretical calculation shows that the midspan is expected to crack when load reaches 3000 lb (13.3 kN) (De Luca et al. 2011). In order to indicate the crack initiation at midspan, the first segment is chosen to cover loading up to 3500 lb (15.6 kN) just above anticipated theoretical midspan cracking load. Loading from 3500 lb (15.6 kN) to failure (9000 lb (40.0 kN)) then is split into two segments for purpose of clarity of analysis. The number of AE events at midspan increases considerably when the load approaches 3100 lb (13.8 kN) (**Fig. 2-8 a)** indicating crack initiation at midspan. **Fig. 2-8 b** shows an increase in the AE event rate, as cracks continue to propagate and form. The last stage (**Fig. 2-8 c**) produces the largest number

of events, which is due to the crack extending and spreading in the center portion of the strip.

Using the AE data between 0 to 9000 lb (40.0 kN) load levels, the cracks (events) identified under the load test are located and an AE crack map for the midspan region is developed. **Fig. 2-9** shows the crack evolution during the loading process. For each load segment, the AE estimated source location of the cracks in the X-Y plane are visualized from the bottom and compared with a picture of cracks taken during the load test (**Fig. 2-9).** The location of AE sources is marked with a square and each circle represents the location of a sensor. The pictures taken in the field are not to scale and cracks lines are manually accentuated on visible cracks for purpose of clarity. As seen in **Fig. 2-9**, located AE events correspond closely to the locations of visible cracks, and often precede their appearance. For instance, in **Fig. 2-9 a** there are cracks located on the right side of sensors 3 and 4 in the AE map which were not visible during the load test in this stage, but later by increasing the load they became visible (**Fig. 2-9 b**).This comparison shows the ability of AE location technique to identify and locate cracks at early stage before they become visible.

In **Fig. 2-9** the accuracy of crack location varies because of two important limitations:

- The presence of cracks affects the velocity of waves traveling from source to sensors.
- The area enclosed by the sensors does not entirely cover the area affected by cracks.

During the test, crack initiation and propagation create barriers for wave to travel across the cracks. Therefore, a wave travels a longer path to reach the sensors and these changes the effective velocity from source to sensor and directly affects the accuracy of crack

location. By introducing the optimal velocity, the error is significantly reduced, but velocity changes during the test and earlier cracks are more precisely located than the final stage cracks. This uncertainty can be seen in **Fig. 2-9 c** where the cracks on the left side of sensors 5 and 6 are not as clear as earlier cracks. Accuracy of location at all stages of the test can be maintained and improved by introducing variable velocity.

The location accuracy is best in the area enclosed by the sensors and decreases as sources move outside this area. Due to the limited number of sensors and material attenuation, only the center part of the strip (**Fig. 2-6**) could be covered with the enclosed array of the sensors, thus affecting accuracy outside this area (**Fig. 2-9 c)**. It should be noted that if the crack occurring outside of enclosed area of the sensors has high source amplitude and energy, it can still be located with good precision (**Fig. 2-9 c**). The results shown in **Fig. 2-9** demonstrate that the proposed approach has the potential for AE crack detection and location in RC members even with a limited number of sensors and simplifying assumptions.

2.5 CONCLUSIONS AND FUTURE WORK

The load test was performed on one way slab strips and the formation and propagation of cracks was observed. A methodology based on error minimization was proposed to capture and locate cracks using correlated AE events. As a result, a number of events highlighting the crack pattern was calculated and mapped. The methodology can be routinely used as pre-test before load testing on RC slabs. Approaches for establishing sensor arrangement, TOA selection, velocity optimization and data filtering were introduced. Sequence of controlled crack propagation, in RC strips was observed and the AE technique was able to locate the cracks with limited number of sensors (i.e., eight per

strip) while they were forming and in some cases before they were visible. The pattern of the located AE events was consistent with the analytical calculations and experimental outcomes. The results show that this method has the potential to be a component of a structural load test.

Additional research is necessary to introduce variable velocity in each stage of the load test for crack location. In addition, future work needs to develop a pattern recognition technique which can automatically recognize and draw the crack lines directly from the AE point locations.

Table 2-1: Summary of as built slab properties.

Short span	12.0 ft (3.66 m)
Long span	24.0 ft (7.32 m)
Thickness	5.0 in. (127 mm)
Effective reinforcement depth (supports)	3.75 in. (95.3 mm)
Effective reinforcement depth (mid-span)	4.25 in. (104 mm)
Concrete strength	3,000 psi (20 MPa)
Steel strength	65,000 psi (448 MPa)
Main reinforcement[*,**]	#5@10 in. (16 @203 mm)
Secondary reinforcement[**]	#3@16 in. (9.5@406 mm)

* Negative moment (top) bars missing at some locations.
** Two layers (top and bottom) of smooth bars.

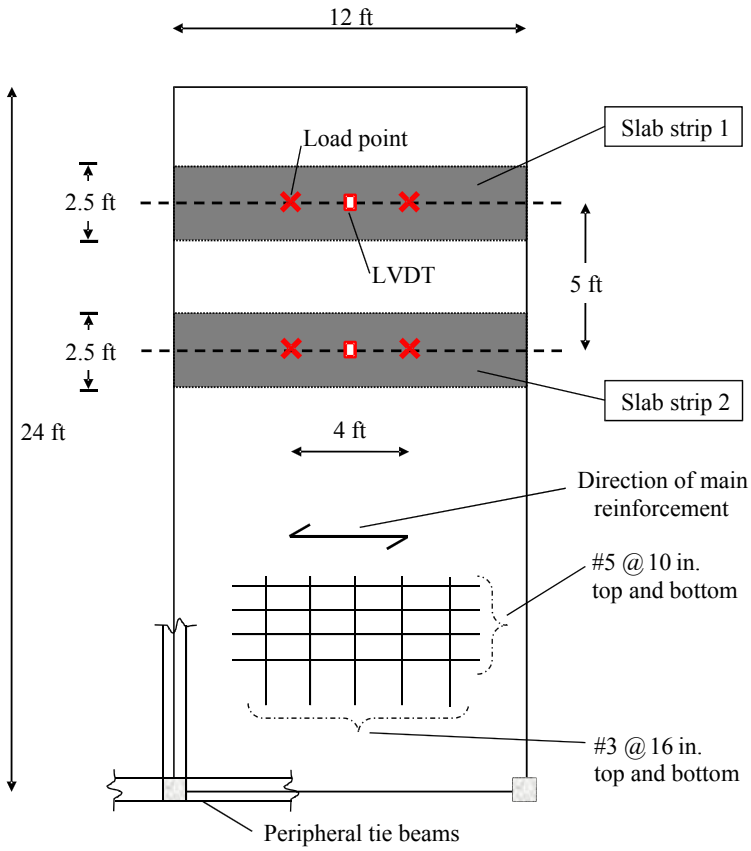

Fig. 2-1. Slab strip layout. (Note: 1 in.=25.4 mm, 1ft=304.8 mm)

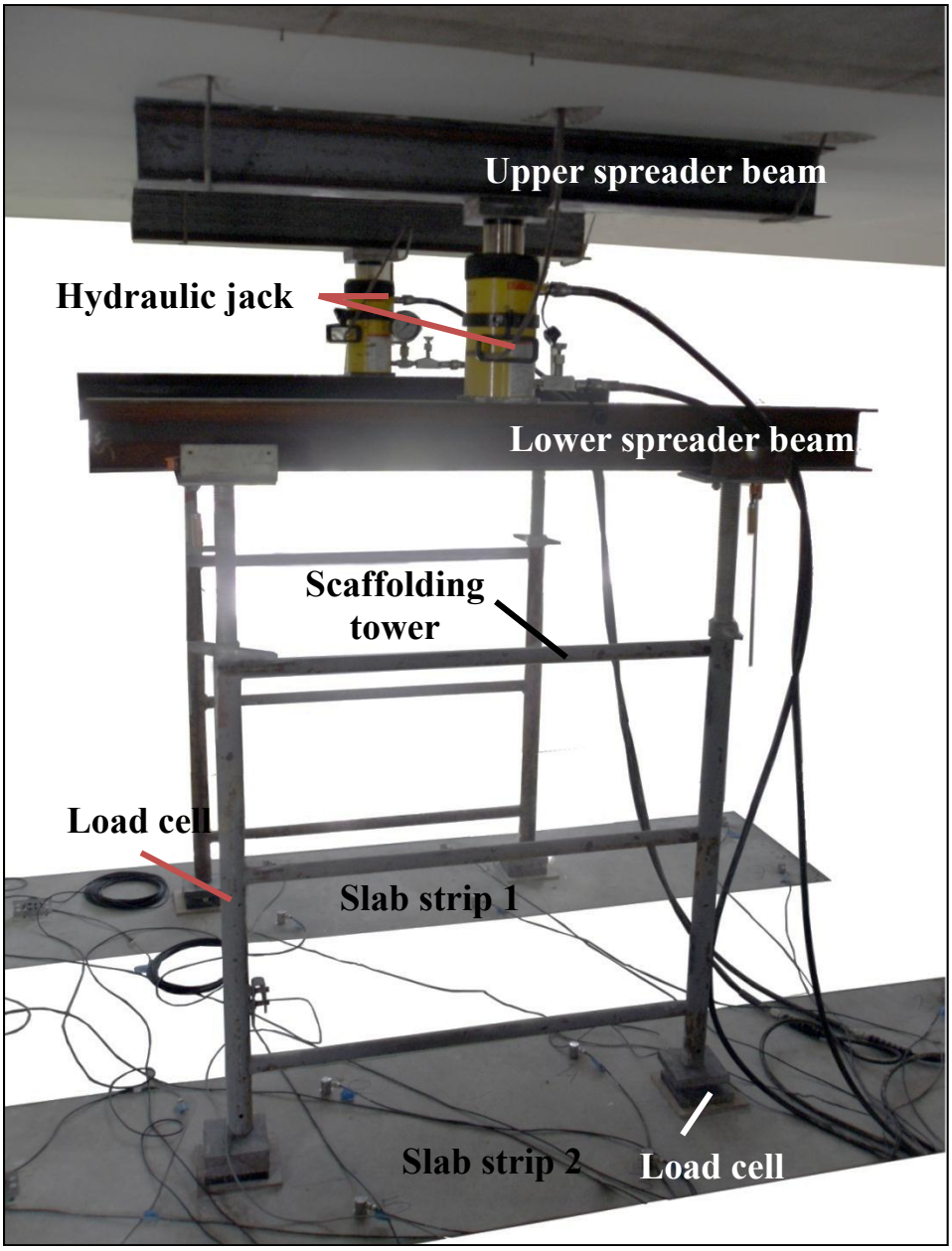

Fig. 2-2. Load test setup.

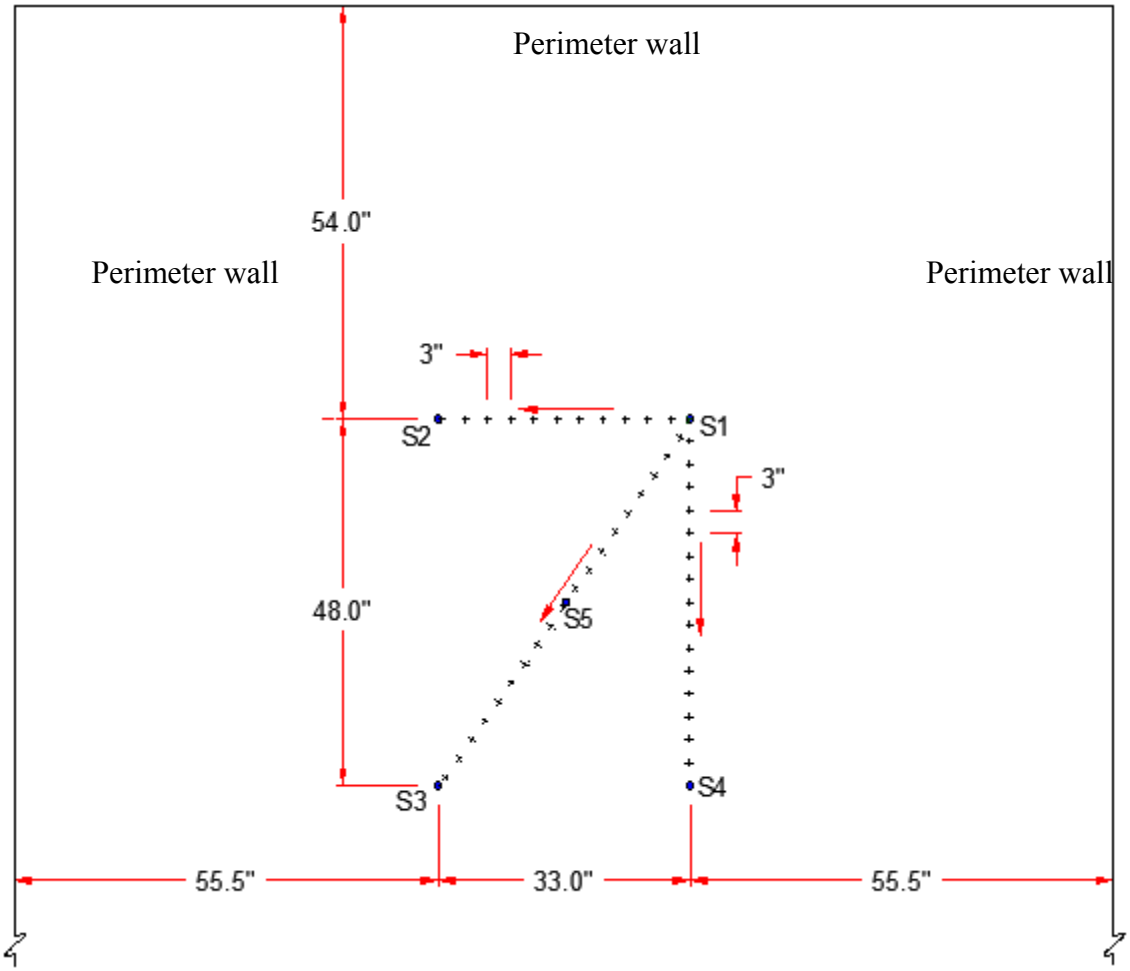

Fig. 2-3. Paths and sensor setup for AE pre-test. (Note: 1 in.=25.4 mm)

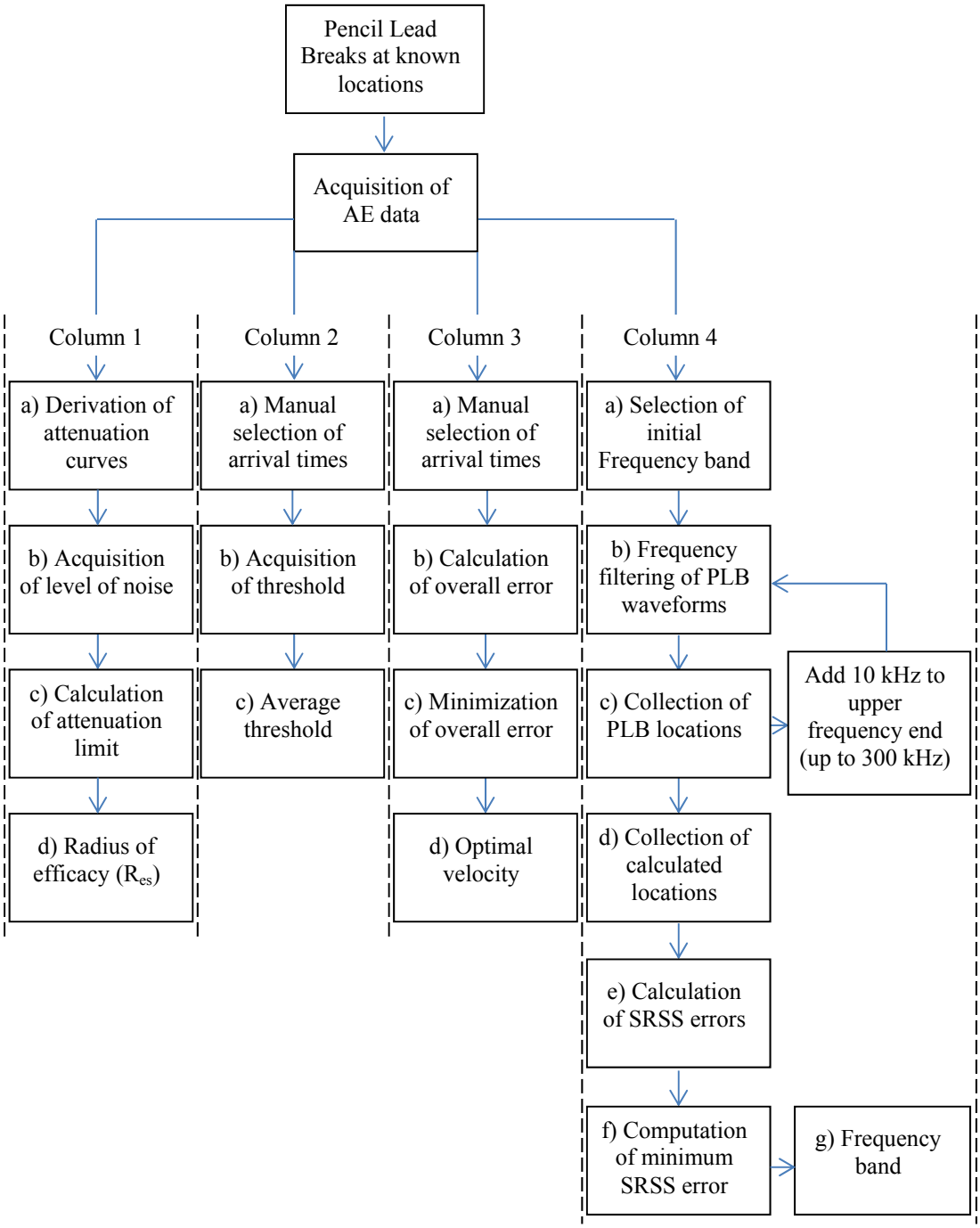

Fig. 2-4. Method of analysis of AE pre-test data

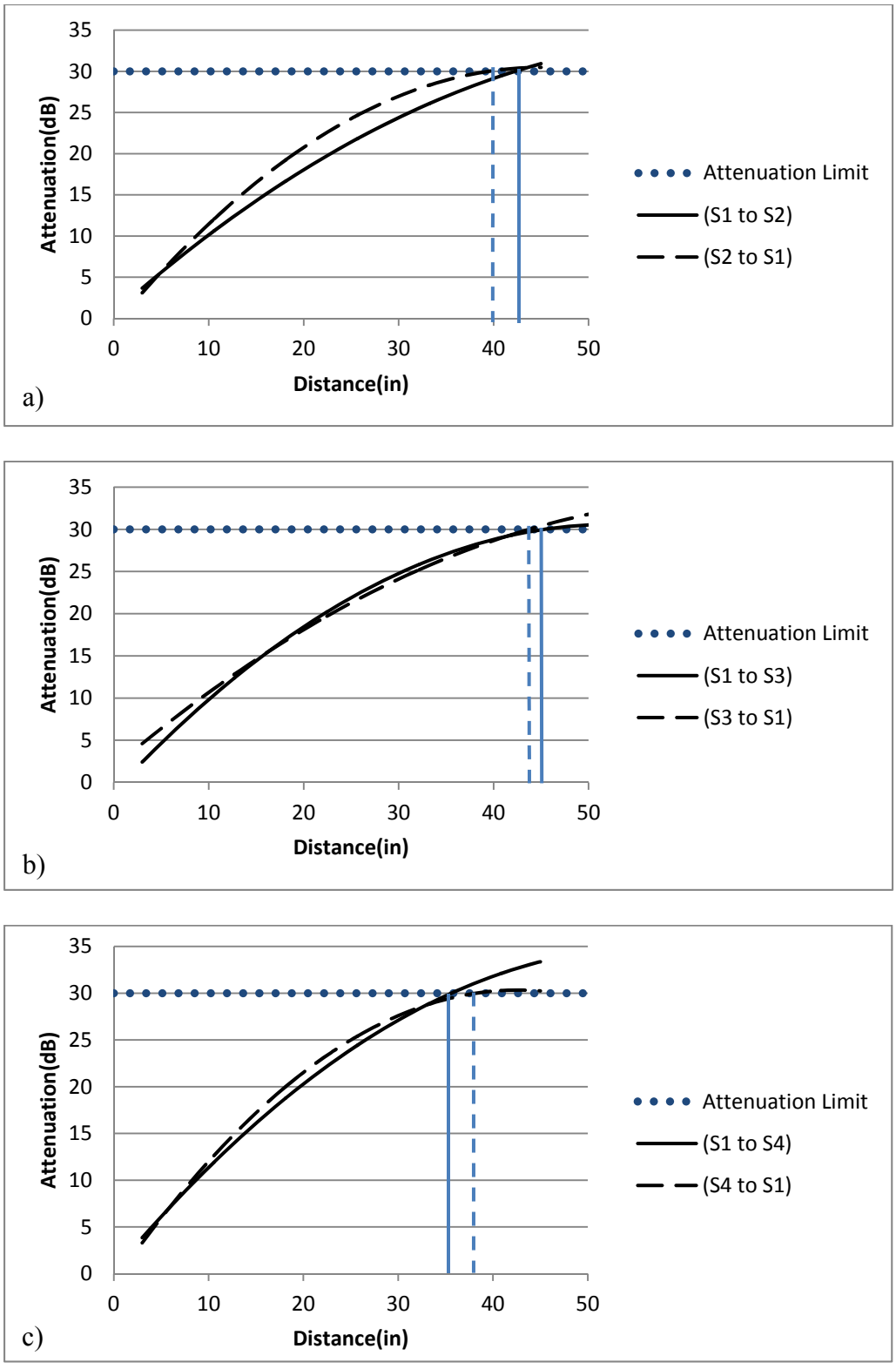

Fig. 2-5. Attenuation curves for selected paths: a) S1-S2 b) S1-S3 c) S1-S4. (Note: 1 in.=25.4 mm)

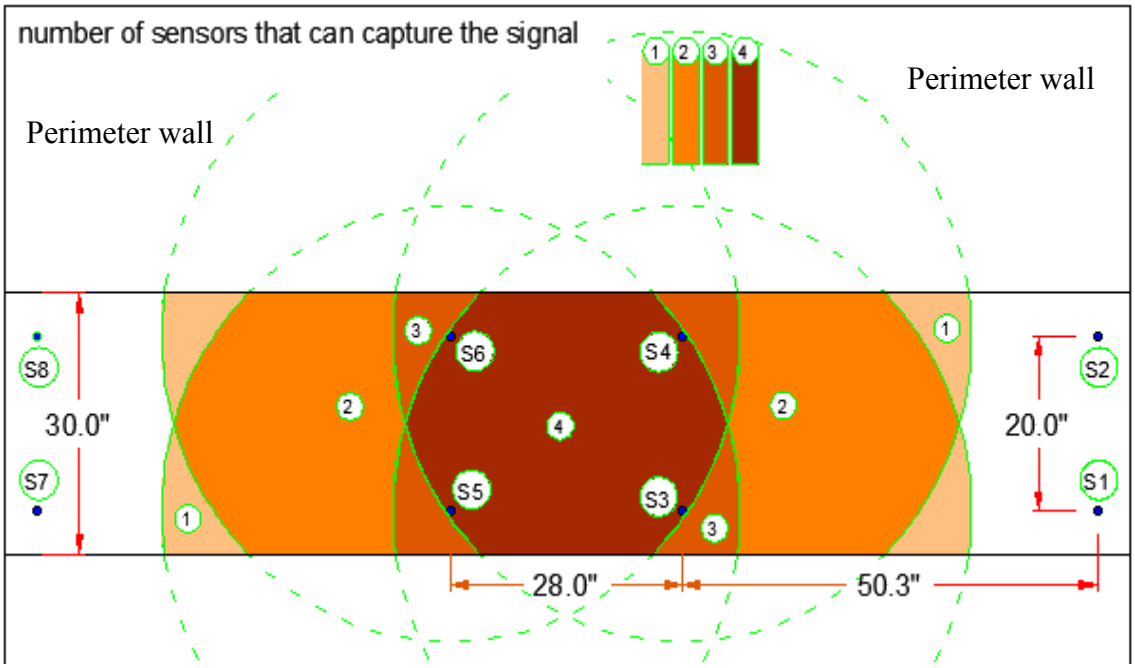

Fig. 2-6. Schematic map of locating capabilities and area of efficiency of the sensors for strip 2.

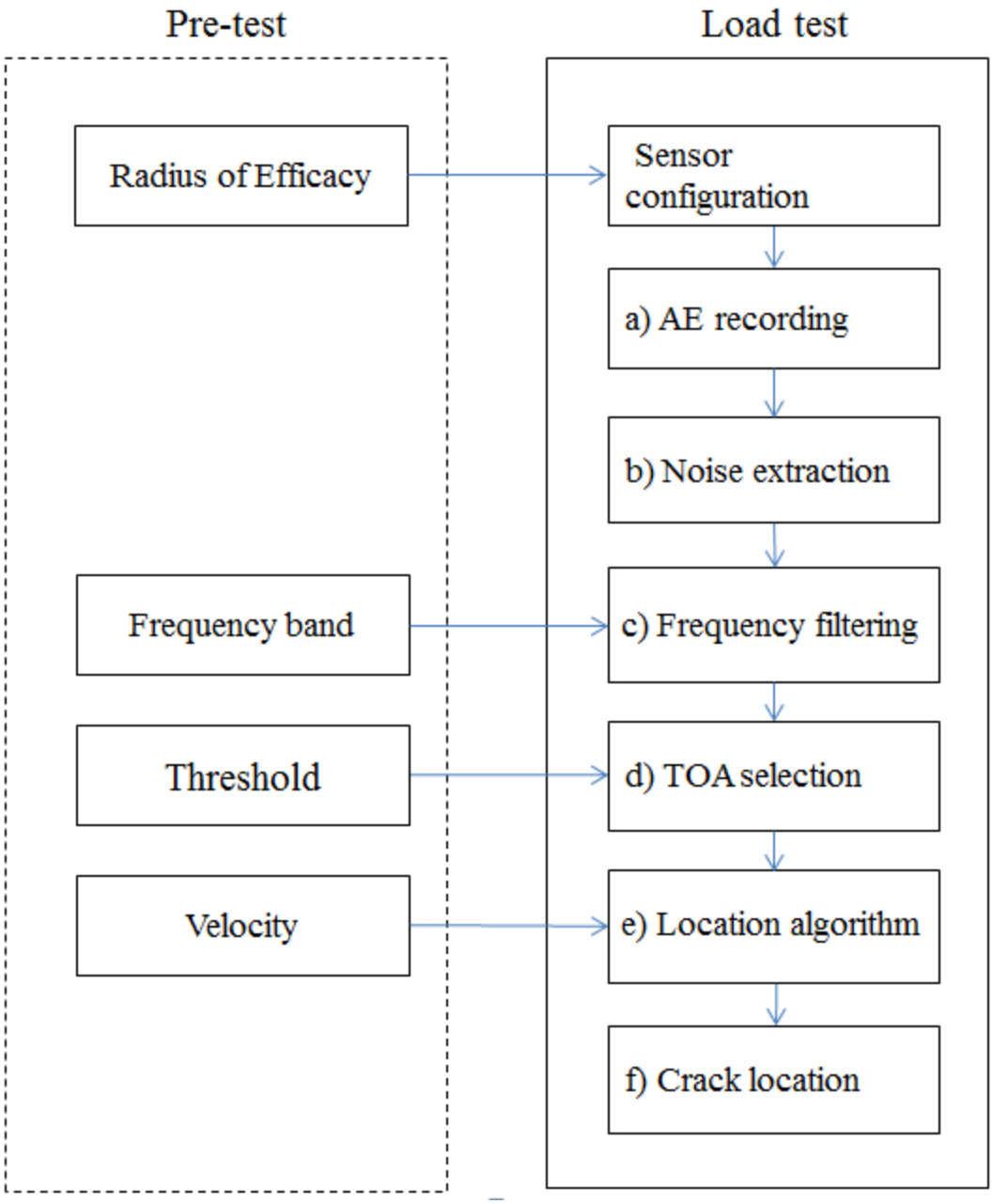

Fig. 2-7. Flow chart of the method of crack location during a load test

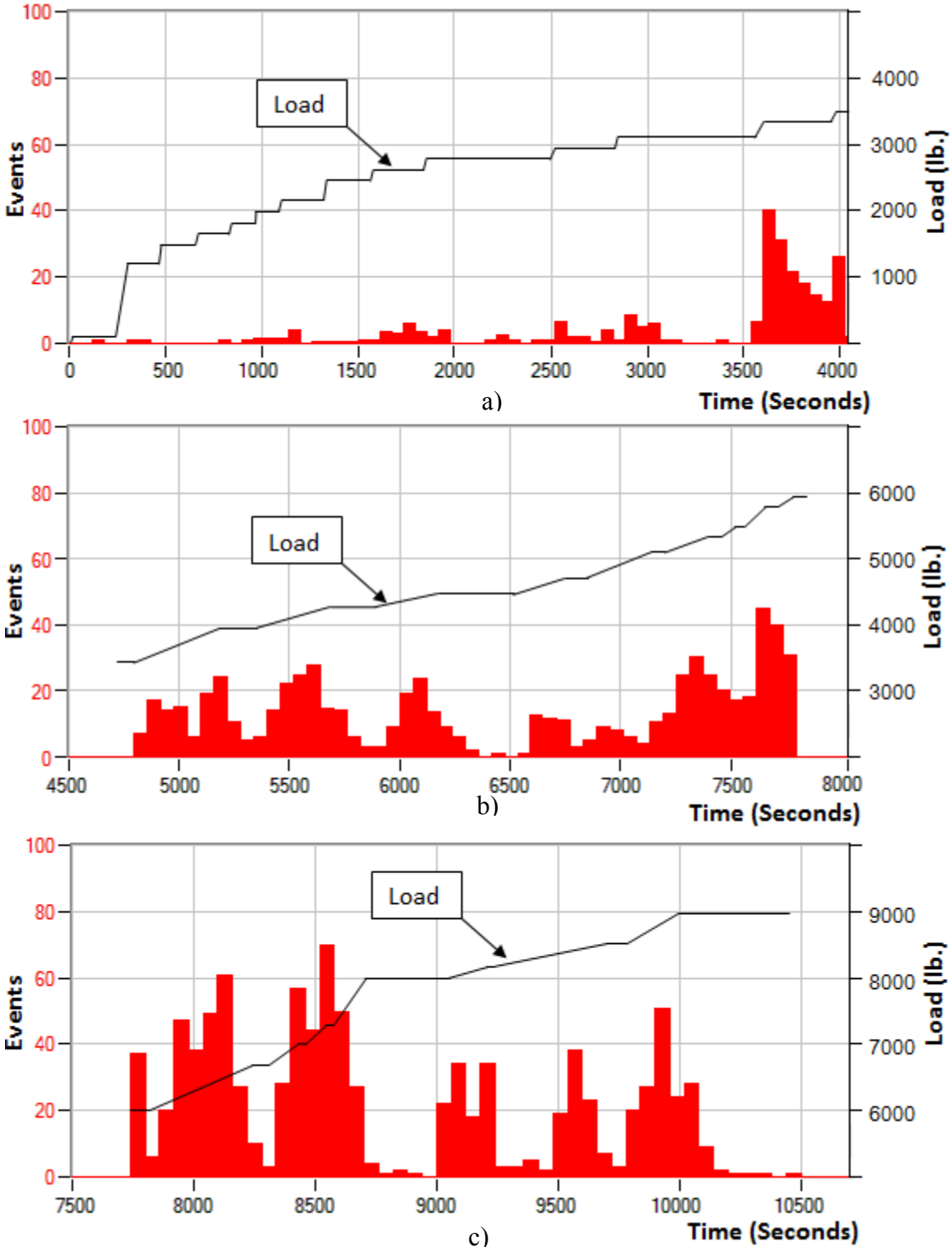

Fig. 2-8. Events vs. time at midspan for loading from : a) 0 to 3500 lb. b) 3500 to 6000 lb. c) 6000 to 9000 lb. (Note: 1,000 lb=4.448 kN)

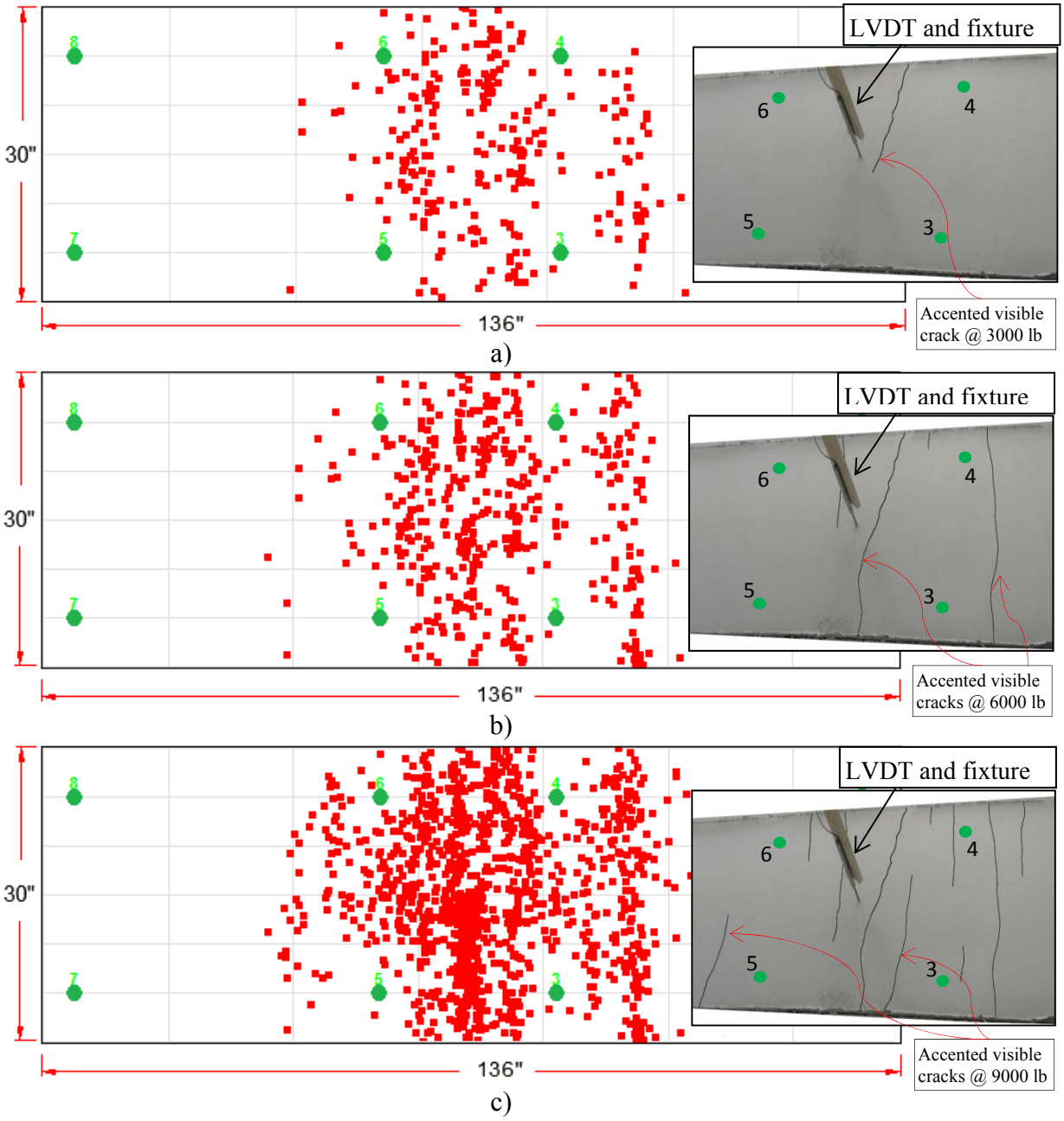

Fig. 2-9. Mid-span crack location for loads up to: a) 3500 lb b) 6000 lb c) 9000 lb. (Note: 1,000 lb=4.448 kN, 1in.=25.4 mm)

CHAPTER 3: STUDY 2 - EXPERIMENTAL STUDY OF ACOUSTIC EMISSION WAVE PROPAGATION IN CONCRETE SLABS

SUMMARY

Various Non-Destructive Testing (NDT) techniques are now available for Structural Health Monitoring (SHM) and Acoustic Emission (AE) is one of them. A potential advantage of the AE technique is its capacity to locate active defects in Reinforced Concrete (RC) members if scattering and attenuation of stress waves could be successfully addressed. Due to the inhomogeneous nature of RC, presence of cracks and complexity of propagating acoustic waves, it is difficult to identify and characterize AE sources and their locations. This research experimentally and analytically studies AE wave propagation and boundary condition effects as a function of slab thickness, concrete strength and concrete constituents. Ten slabs with variable parameters including strength, unit weight, aggregate size, aggregate type, geometry and presence of steel reinforcement were cast. AE signals were generated at known locations on the slab surface using Pencil Lead Breaks (PLBs), an ASTM standard method, and recorded by four AE sensors. Results confirm the effects of the above-named parameters on attenuation and velocity of acoustic waves. The outcomes of this research can be used to develop a reference database for AE wave attenuation and velocity applicable in the field for SHM of concrete members.

BACKGROUND

The aim of this study is to experimentally characterize the role of concrete constituents and geometry in AE wave propagation in slabs. Accordingly, slabs with variable parameters including strength, unit weight, aggregate size, aggregate type, geometry and presence of steel reinforcement were cast to allow exploring attenuation and velocity of AE waves. A procedure to calculate AE wave velocity in RC members is introduced and the effect of waveform analysis on velocity determination is investigated. Results obtained from this study are utilized to provide information on wave attenuation and velocity in concrete slabs in form of reference tables which can be applicable for AE in-situ tests and SHM purposes.

3.1 RESEARCH SIGNIFICANCE

This study investigates the relationship between AE wave propagation (attenuation and velocity) and concrete parameters (constituents and geometries). A methodology to measure optimized wave velocity propagating through concrete slabs is developed. The overarching goal is to provide a reference database for AE wave attenuation and velocity for concrete elements relevant to in-situ applications.

3.2 ACOUSTIC EMISSION OVERVIEW

AE terminologies used in this paper are briefly defined in this section. AE is a phenomenon of transient stress waves resulting from a sudden release of elastic energy caused by mechanical deformations, initiation and propagation of microcracks, dislocation movement and other irreversible changes in material (ASTM E1316 2010).

These waves can be detected on the surface of specimens or structures by piezoelectric transducers which convert the mechanical vibrations to electric signals (AE signals). A signal that exceeds a defined threshold is called a "*hit*" and exceeding the defined threshold triggers the accumulation of data. If the same signal is recorded by more than one sensor, it is considered to be illustrative of a significant incident and is called an "*event*". Events can be recorded and analyzed to obtain further information regarding the source of the signals (Carpinteri et al. 2008). Two fundamental concepts of AE wave propagation which are investigated in this study are "*wave attenuation*" and "*velocity*".

3.2.1 Wave Attenuation

Attenuation dampens a stress wave as the wave front propagates away from its source and spreads over a larger volume. Attenuation of a stress wave in an infinite medium causes the wave amplitude to decrease proportional to the distance from the wave source (Miller and Mclntire 1987). RC has unique characteristics due to heterogeneity, porosity and presence of cracks and steel reinforcement. Besides internal damping, AE waves travelling in RC members undergo reflection, scattering, mode conversion and diffraction, all of which influence the propagation of stress waves (Miller and Mclntire 1987 and Al-Wardany et al. 2007). Wave attenuation limits sensor distance, which, in turn, limits the area that can be accurately monitored by a fixed number of sensors (Guratzsch and Mahadevan 2010). Therefore, attenuation is considered as having the major influence on the accuracy of data collected from RC members.

3.2.2 Wave Velocity

Knowledge of wave velocity is critical for AE source location. The most commonly used AE location method is known as the Time of Arrival (TOA) method, where the location of the damage can be determined from the TOA of the event at two or more sensors (Salinas et al. 2010). When using TOA method, the velocity of the wave that propagates through the material needs to be known. An inaccurate assumption of wave velocity can contribute to large errors in source location (Muhamad Bunnori et al. 2006). Homogenous materials have well defined velocities, but this is not the case for inhomogeneous materials such as concrete. The basis for the wave velocity calculation is the time-distance relationship implied by the velocity of the wave. The absolute arrival time, t, of a hit in an event can be combined with the velocity of the AE wave, v, to yield the distance, d, from the sensor to the source:

$$d = vt \tag{3-1}$$

In this equation, the distance d_i between the source of AE wave coordinates (x_0, y_0, z_0) and sensor i with known coordinates (x_i, y_i, z_i) can be found as:

$$d_i = \sqrt{(x_i - x_0)^2 + (y_i - y_0)^2 + (z_i - z_0)^2} \tag{3-2}$$

The distance of the source to the sensor "i" can also be given by:

$$d_i = v(t_i - t_0) \tag{3-3}$$

Where t_i is the TOA to the sensor i and t_0 is the time of event occurrence.

If the coordinates (x_0, y_0, z_0) of the source of AE wave is known, by determining TOA of the AE wave, the velocity can be calculated (Salinas et al. 2010). Because of the presence of surfaces, several modes of wave propagation exist within a body. Compression (P)

waves mostly are used for source location and velocity calculation (Muhamad Bunnori et al. 2006 and Grosse and Finck 2006). Estimating the correct TOA for the P wave is a challenge especially when a wave propagates through concrete. The automatic determination of TOA can be based on a present threshold (in dB scale) which is specific to a particular material and transducer (Ding et al. 2004). TOA is calculated from the first signal excursion above the threshold. Therefore, the choice of the threshold value is crucial to the quality of the TOA selection and velocity results.

3.3 EXPERIMENTAL PROCEDURE

In this investigation ten concrete slabs (C1-C10) with six variable parameters including compressive strength, unit weight, aggregate size, aggregate type, thickness and presence of steel reinforcement were manufactured (see **Table 3-1**). The dimension of each slab was 3.0 x 4.0 ft. (91.4 x 121.9 cm) with thicknesses of 4 to 12 in. (102 to 305 mm) (**Table 3-1**). The compressive strength of concrete used for each slab was measured by testing three 8 x 4 in. (203 x 102 mm) cylinders at 3, 7, 14 and 28 days of age according to ASTM C39 specifications (ASTM C39 2010). The mixture design of each slab is shown in **Table 3-2**. The steel reinforcement layout for the RC slab (C9) is shown in **Fig. 3-1**. In order to investigate AE signal propagation under a Saturated Surface-Dry (SSD) condition, light-weight aggregate slab (C2), after conducting the AE planned tests at 28 days, was stored in water for two months and the AE test repeated under SSD condition (C10). Concrete cylinders stored in the similar condition were used to measure water absorption.

3.3.1 AE Equipment

PAC Sensor Highway II system (AEwin Software User's Manual 2009) equipped with R6I-AST resonance sensors is used for AE data collection. The R6I-AST resonance sensors have an operating frequency range of 40 - 100 kHz and a resonant frequency of 55 kHz. The "I" designation indicates that the sensor has a built-in 40 dB preamplifier. To ensure proper coupling of each AE sensor, a two-part epoxy contact agent was applied to connect the sensors to the concrete surface.

3.3.2 AE Setup and Measurements

The AE tests are performed on each slab surface by Pencil Lead Breaks (PLBs) at given locations to generate acoustic waves while the sensors are recording the signals. PLB is an ASTM standard method to produce similar AE events (ASTM E 976 2010). In order to investigate the AE wave propagation PLB tests were performed together with compressive strength tests, at 3, 7, 14 and 28 days after the specimens were cast. The arrangement of the sensors for the AE test is given in **Fig. 3-2**. Four sensors are placed in a rectangular fashion for the wave attenuation and velocity to be investigated in three directions. Using the standard 0.5 mm (0.019 in.) diameter lead, PLBs were conducted at 3 in. (76.2 mm) intervals between the sensors along the lines S_1-S_2; S_1-S_3; and S_1-S_4 (**Fig. 3-2**). In order to minimize and uniformly distribute the operator errors, the PLBs were repeated three times at each position following a fully randomized order.

3.4 EXPERIMENTAL OBSERVATIONS AND RESULTS

3.4.1 Wave Attenuation

Fig. 3-3 shows an example of six attenuation curves derived for the three PLB paths shown in **Fig. 3-2** for slab C8 at 28 days of age. Similar graphs were created at various concrete ages and for all slabs. **Fig. 3-3 a** shows the attenuation curves for the three paths using the data recorded at sensor S_1. **Fig. 3-3 b** shows the same three curves using the collected AE data from sensors S_2, S_3 and S_4. These two graphs are in the format of amplitude vs. distance where the drop of amplitude at a certain distance from the recording sensor represents the attenuation over that distance. Each point represents the average of three PLBs repetitions. For all specimens, the maximum average difference in amplitude, with similar sensor to source distance, among three paths is about 4 dB that is considered to be not highly significant and the result of the nature of concrete. For the remaining diagrams shown in this paper the path S_1-S_3 (S_1 recording sensor) is used since it is the longest path tested.

The attenuation curves for slabs C4 and C7 are shown in **Fig. 3-4 a** and **b**, respectively, for tests at ages 3, 7, 14 and 28 days. As expected, attenuation decreases as a function of maturity and this phenomenon is more pronounced for lower strength concrete. This trend was manifested by all specimens. Similarly, **Fig. 3-5** shows the attenuation curves for five slabs (C2, C4, C5, C6 and C10) at the age of 28 days. It is observed that:

- C2 and C4 indicate that lightweight concrete is significantly more attenuative than normal weight concrete. As expected, density affects attenuation.
- C4, C5 and C6 indicate that the 28-days concrete strength (i.e., 3,290 vs. 6,745) has no impact on AE signal attenuation.

- C2 and C10 (the same slab) indicate that the AE signal is less attenuated in the saturated surface-dry condition.

Fig. 3-6 shows the attenuation curves for five slabs (C4, C5, C7 and C8) at the age of 28 days. It is observed that:

- C5 and C7 show that aggregate size has little effect on the signal attenuation
- C4 and C8 with crushed and natural aggregate and comparable compressive strength, indicate that the aggregate type has a significant impact.

Also, from the remaining tested slabs it is observed that:

- C9 and the plain concrete slab with the similar compressive strength C4 indicate that the existence of steel reinforcement increases the signal attenuation.
- C1 to C3 indicate that by enlarging the slab thickness the attenuation increases. This implies that the geometry of structure has direct effect on signal attenuation.

The results from all attenuation tests are utilized to develop a reference table for AE monitoring of an RC structure, which can provide guidance about the member's attenuation especially when sensor spacing and source location are concerned (**Table 3-3**).

3.4.2 Wave Velocity

For each slab the wave velocity is derived for three PLB paths of **Fig. 3-2** at concrete ages of 3, 7, 14 and 28 days. In order to investigate the effect of threshold level on calculated p wave velocity, three low threshold levels (i.e., 30, 35 and 40 dB) are utilized for velocity calculation.

3.4.3 Methodology

For each path there is a minimum of 33 PLB events that can be used to obtain the velocity. Since the basic velocity calculation is applied to a single event, an optimization procedure to calculate wave velocity can be implemented. The procedure developed to calculate the optimal wave velocity through the slab under consideration consists of these steps:

a) Selecting the TOAs

b) Defining the overall error based on calculated and known locations of the PLBs

c) Minimizing the overall error

d) Finding the optimal velocity

In step (a), waveforms recorded from PLBs performed between the sensors (**Fig. 3-2**) are used for TOA selection. For each line (S_1-S_2, S_1-S_3, S_1-S_4), the TOAs of each PLB located on that line to the end sensors are selected automatically based on their waveforms. The automatic determination of TOA is based on a present threshold (in dB scale). TOA is calculated from the first signal excursion above the threshold. In this procedure three threshold levels (30, 35 and 40 dB) are considered to determine the TOA for each signal.

In step (b) and (c), the optimal velocity is defined so that the overall error, E_D, between the difference of calculated distances $\Delta d_j = (d_2 - d_1)_j$ of PLB j to the end sensors and their actual values, $\Delta D_j = (D_2 - D_1)_j$, is minimized. For each break located between the sensors along the lines S_1-S_2, S_1-S_3, and S_1-S_4 (**Fig. 3-2**), d_2 and d_1 are the calculated distances of PLB j to the end sensors and D_2 and D_1 are the exact distances. Defining the error as:

$$E_D^2 = \sum_{j=1}^{n} \left(\Delta D_j - \Delta d_j\right)^2 = \sum_{j=1}^{n} \left(\Delta D_j - v\Delta t_j\right)^2 \quad (3\text{-}4)$$

Where $\Delta t_j = (t_2 - t_1)_j$ and the automatically recorded arrival times of PLB j to the end sensors are t_1 and t_2 .The overall error can be minimized by:

$$\frac{\partial E_D^2}{\partial v} = 0 \rightarrow \sum_{j=1}^{n} \Delta t_j (\Delta D_j - v \Delta t_j) = 0 \quad (3\text{-}5)$$

Resulting in the optimal velocity, v of:

$$v = \frac{\sum_{j=1}^{n} \Delta t_j \Delta D_j}{\sum_{j=1}^{n} \Delta t_j^{\,2}} \quad (3\text{-}6)$$

In step (d), by substituting all TOAs selected in step (a) and known location of PLBs in Eq. (3-6) the optimal velocity is calculated.

3.4.4 Results

It is clearly observed that the wave velocity is not constant over every path in the concrete slabs and it changes up to 5000 in/s (*127*.0 m/s), and thus it can be deducted that the velocity in concrete slab is path dependent. It should be noted that a relatively small change of 1000 in/s (25.4 m/s) in the magnitude of velocity over 1 millisecond period can cause an inch of change in the estimation of distance traveled by the wave. In order to compare wave velocities for different slabs shown in **Table 3-1**, the average velocity of three paths is considered. The results illustrate significant growth in wave velocity comparing 3 to 7 days of concrete age. After 7 days, although a slight increase in the wave velocity can be observed, it remains mainly constant. This can be attributed to the fact that 60-70 percent of compressive strength of all specimens is gained in the first 7 days after casting. For this reason the data for presentation are divided to two parts: 3 and 28 days of concrete age (**Table 3-4**). In order to understand effect of threshold in velocity calculations, results calculated for three threshold levels are presented in **Table 3-4** for

slabs at 28 days**.** For sake of brevity, only the results obtained for threshold of 35 is presented for slab of 3 days age. The main observations and conclusions can be summarized as follows:

- Wave velocity is dependent upon the threshold level, higher threshold levels prolong the TOA of the wave and the velocity is reduced.
- Wave velocity in concrete varies from 90,000 in/s (2286 m/s) to 160,000 in/s (4064 m/s) depending upon threshold level, concrete composition, compressive strength and geometry.
- Wave velocity is dependent on 28 days concrete compressive strength, the increase of which increases the velocity.
- By comparing the wave velocities for two slabs with different maximum aggregate size and similar compressive strength (C5 and C7), it is concluded that aggregate size has an inverse effect on the wave velocity, as the aggregate size increases the wave velocity decreases.
- Comparing slabs C5 and C8, it is found that the wave velocity for the crushed aggregate slab is higher than that of the natural aggregate slab with similar geometry and compressive strength.
- The results obtained from slabs C1 to C3 indicate that the slab thickness has a direct effect on wave velocity and by enlarging the slab thickness the velocity decreases.
- The results obtained from slabs C4 and C9, with similar geometry and compressive strength point out that existence of top reinforcement increases the wave velocity. It should be noted that this result is for the slab with cover thickness and steel bar spacing presented in **Fig. 3-1**.

- Comparing slabs C2 and C4, it is found that the wave velocity for the lightweight slab is higher than that of the normal weight slab with similar geometry and compressive strength.
- The wave travels with a much lower velocity in the concrete with the saturated surface dry condition (comparing specimens C2 and C10). This is attributable to the presence of water in the media which slows the wave.

The velocity results from all slabs are utilized to develop a reference table for AE monitoring of RC structure, which can provide proper information about the wave velocity in different RC members especially when source location and filtering are concerned (**Table 3-5**).

3.5 CONCLUSIONS

A set of AE experiments are conducted on the concrete slabs in order to identify the influence of variable parameters including strength, unit weight, aggregate size, aggregate type, geometry, moisture and presence of steel on wave velocity and attenuation. A methodology is developed to assess the optimal wave velocity using PLB tests in each slab. Reference tables for wave attenuation and velocity for AE monitoring application in concrete members are developed. Considering the results of the tests conducted the following conclusions are made:

1. With maturing, velocity increases while attenuation decreases in concrete;
2. 28 days concrete strength seems not to have an influence on the attenuation, but AE signals have a higher velocity through concrete members with higher concrete strength;

3. While concrete aggregate size does not affect attenuation, increasing the aggregate size decreases the wave velocity;
4. Using lightweight and natural aggregates increases attenuation and decreases velocity significantly;
5. Wave velocity for the lightweight concrete is higher than that of normal weight concrete with similar compressive strength;
6. Presence of steel reinforcement increases the signal attenuation and velocity;
7. Attenuation increases with slab thickness while velocity decreases;
8. In saturated surface-dry condition, AE signal has less attenuation and the wave travels with much less velocity; and
9. After 7 days of curing, although a slight increase in velocity can be observed, velocity can be considered constant.

Table 3-1: Concrete slabs specifications.

Slab code	Slab thickness (in.)	Nominal strength (psi)	Nominal unit weight (lb/ft^3)	Max. aggregate size (in.)	Coarse aggregate type	28-day strength (psi)
C1	4	3,000	110	1/2	Lightweight	3,017
C2	6	3,000	110	1/2	Lightweight	3,017
C3	12	3,000	110	1/2	Lightweight	3,017
C4	6	3,000	140	1/2	Crushed	3,920
C5	6	5,000	140	1/2	Crushed	5,351
C6	6	10,000	140	1/2	Crushed	10,070
C7	6	6,000	140	3/2	Crushed	6,745
C8	6	5,000	140	1	Natural	4,838
C9*	6	4,000	140	1/2	Crushed	3,755
C10**	6	3,000	110	1/2	Lightweight	3,017

1000 psi = 6.9 MPa, 1 in. = 25.4 mm, 1 lb/ft^3 = 16.02 Kg/m^3

* Slab reinforced with details shown in **Fig 1**.

** Slab C10 is slab C2 stored in water for two months. 8 by 4 in. cylinders stored in the same condition and had 2.45 % water absorption.

Table 3-2: Concrete slabs constituents.

Slab	Coarse aggregate (lb/yd^3)	Fine aggregate (lb/yd^3)	Cement (lb/yd^3)	Water reducer (oz/yd^3)	Water (lb/yd^3)	Slump (in.)	W/C
C1-C3	1,120	1,140	538	31	167	5	0.31
C4	818	2,103	571	35	314	5	0.54
C5	900	1,777	755	30	342	5	0.45
C6*	1,500	1,360	850	34	86	7	0.10
C7	1,660	1,420	600	30	123	5	0.20
C8	1,550	1,482	500	14	250	4	0.50
C9	860	2,031	570	0	321	5	0.56

1 lb/yd^3 = 0.59 Kg/m^3, 1 in. = 25.4 mm, 1 oz/yd^3 = 0.037 Kg/m^3

* Slab had additional 65 oz/yd^3 super plasticizer in the mixture.

Table 3-3: Reference attenuation for concrete slabs.

Concrete type	Attenuation (dB)				
	Source distance (in.)				
	10	**20**	**30**	**40**	**50**
Normal-weight/Crushed aggregate	9	15	19	21	23
Normal-weight/Natural aggregate	14	20	25	27	29
Light-weight	15	25	29	32	35

1 in. = 25.4 mm

Note:

Listed values are independent of concrete compressive strength and maximum aggregate size and applicable to slabs with less than 6 in. thickness and no reinforcement. Corrections to listed values are as follows:

a) RC, add 6 dB

b) Thickness 6 in. to 12 in., add 5 dB

c) Concrete in SSD condition, subtract 8 dB

Table 3-4: Comparison of wave velocity results.

Slab	Velocity x 10^{-5} (in/s)			
	Day 3*	Day 28*		
	Threshold level (dB)			
	35	**30**	**35**	**40**
C1	1.24	1.36	1.34	1.26
C2	1.20	1.35	1.33	1.25
C3	1.13	1.31	1.27	1.23
C4	1.09	1.19	1.14	1.06
C5	1.14	1.44	1.37	1.24
C6	1.40	1.56	1.49	1.34
C7	1.28	1.47	1.36	1.22
C8	1.11	1.37	1.31	1.15
C9	1.09	1.28	1.22	1.14
C10	Not/App	1.24	1.20	1.15

1 in/s = 0.025 m/s

* Average values for three directions.

Table 3-5: Reference velocity for concrete slabs.

Concrete compressive strength (psi)	Velocity x 10^{-5} (in/s)		
	Threshold level (dB)		
	30	35	40
< 4000	1.19	1.14	1.06
4000 < < 7000	1.44	1.37	1.24
7000 <	1.56	1.49	1.34

1000 psi = 6.9 MPa, 1 in. = 25.4 mm

Note:

Listed values are applicable to slabs with normal-weight concrete, crushed aggregate, ½ in. maximum aggregate size, less than 6 in. thickness and no reinforcement. For other conditions correction to listed values are as follows:

a) Light-weight concrete, add 0.18 in/s

b) RC, add 0.08 in/s

c) Thickness 6 in. to 12 in., subtract 0.05 in/s

c) Concrete with aggregate size larger than ½ in., subtract 0.01 in/s

e) Concrete with natural aggregate, subtract 0.07 in/s

c) Concrete in SSD condition, subtract 0.13 in/s

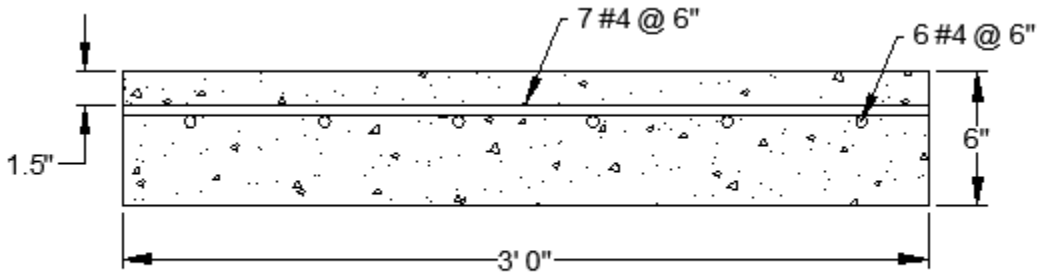

Fig. 3-1. RC specimen layout. (Note: 1 in.=25.4 mm, 1ft=304.8 mm)

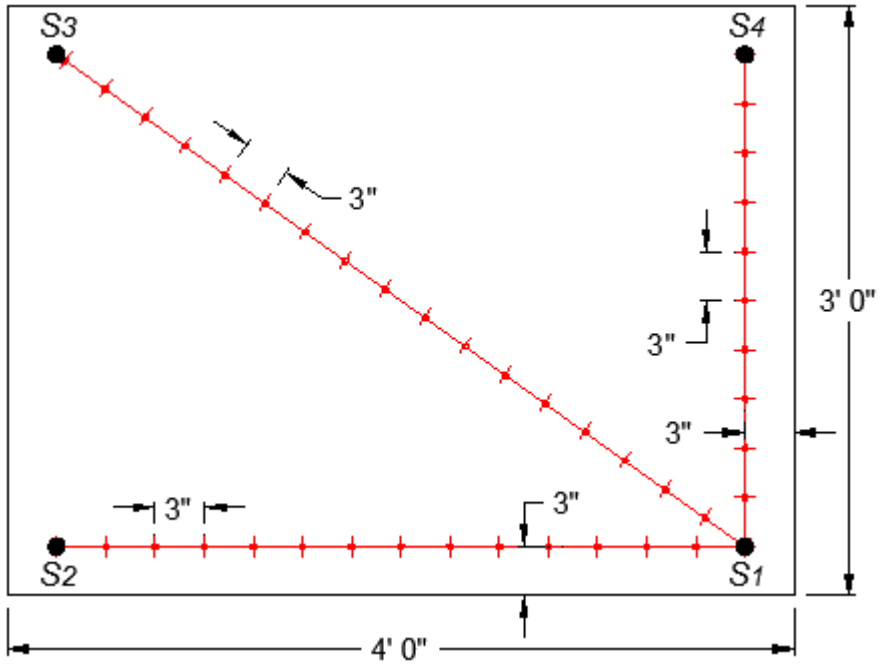

Fig. 3-2. Paths and sensor setup for AE test. (Note: 1 in.=25.4 mm, 1ft=304.8 mm)

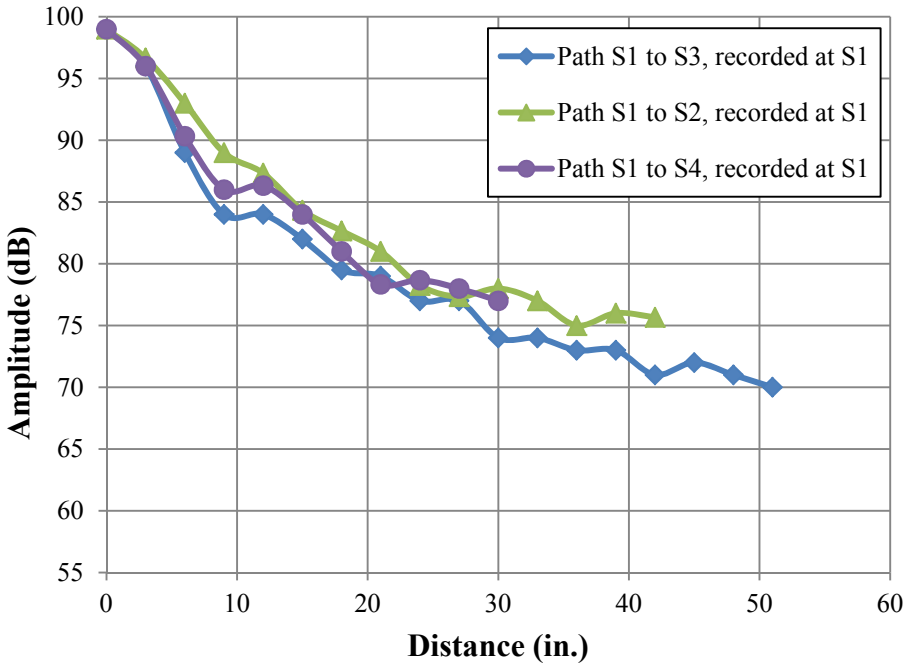

a)

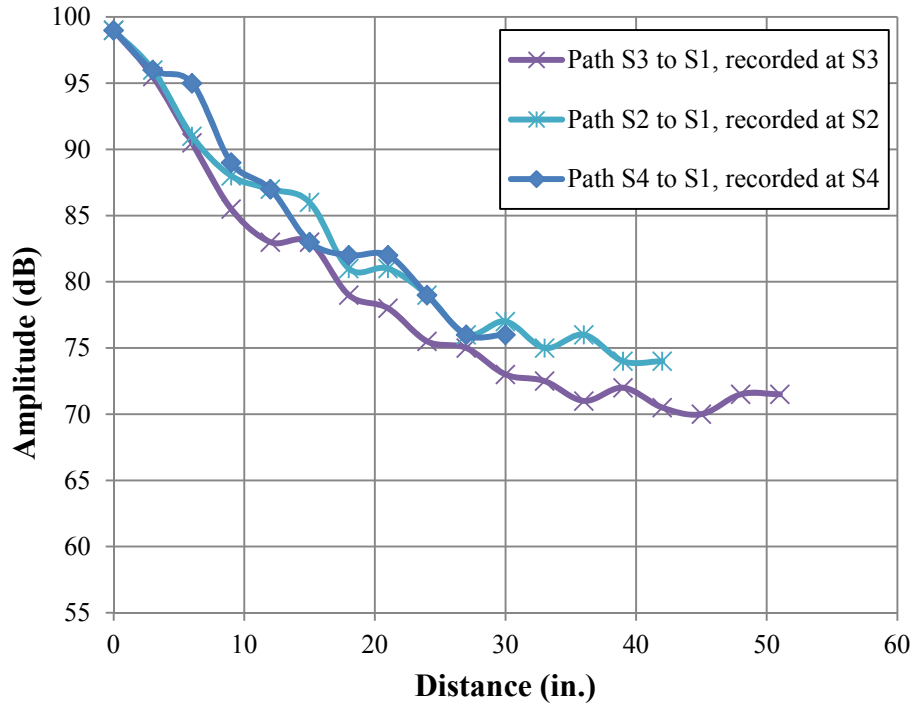

b)

Fig. 3-3. Attenuation curves of slab C8 in different directions at 28 days. (Note: 1 in.=25.4 mm)

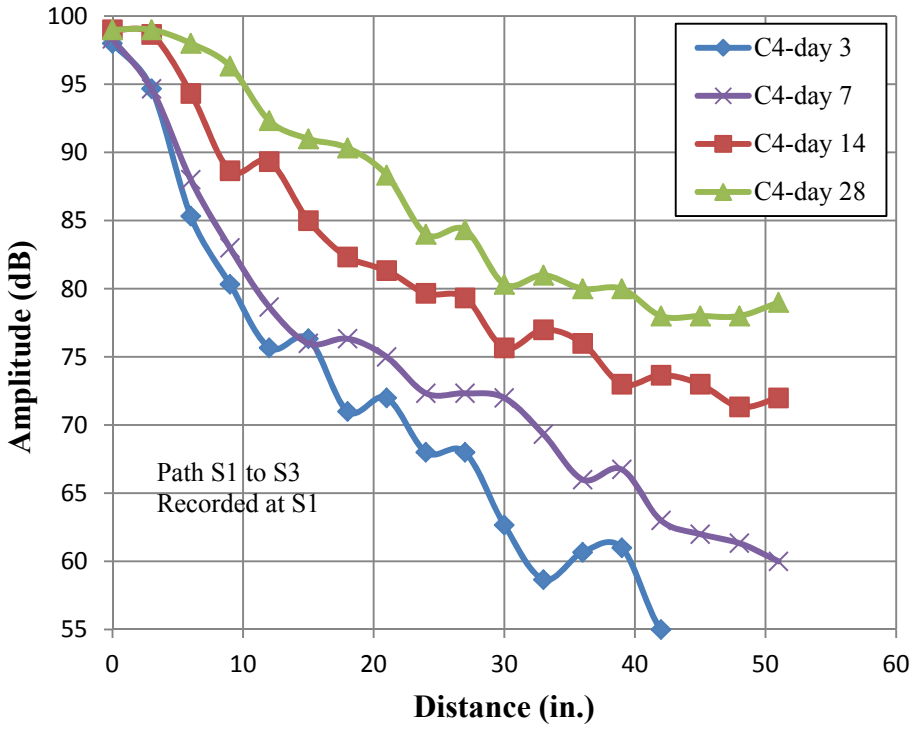

a)

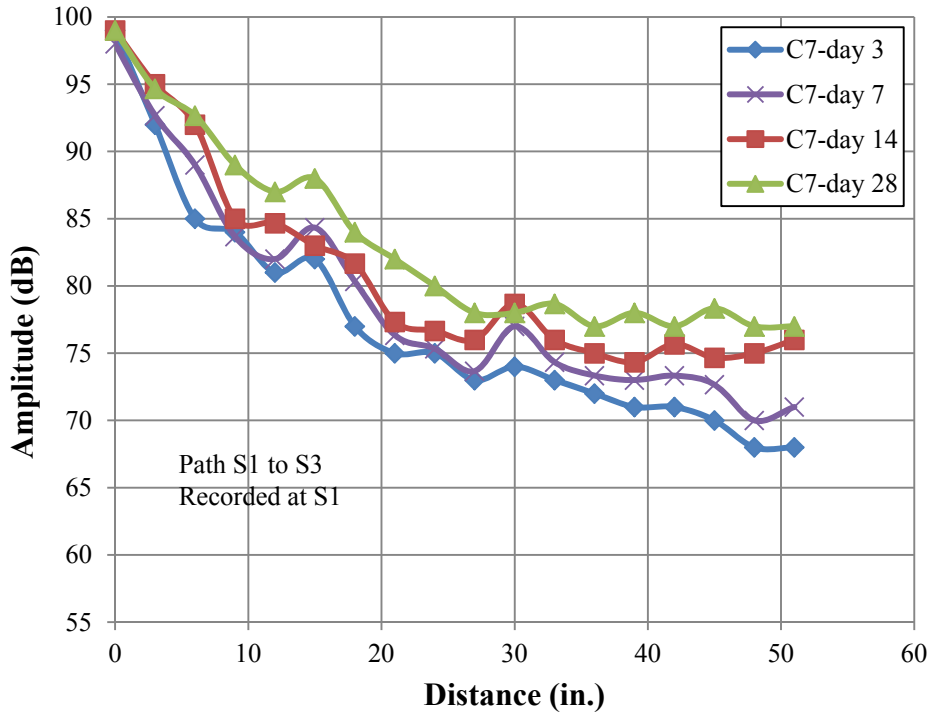

b)

Fig. 3-4. Attenuation curves for selected ages of slabs: a) C4 b) C7 (Note: 1 in.=25.4 mm)

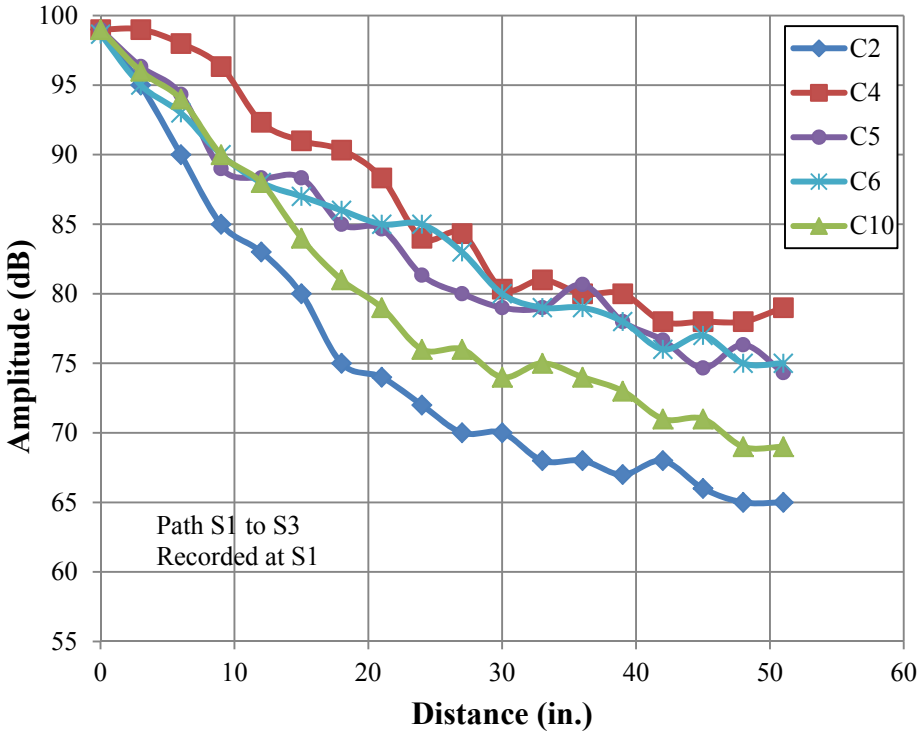

Fig. 3-5. Attenuation curves at 28 days for slabs C2, C4, C5, C6 and C10. (Note: 1 in.=25.4mm)

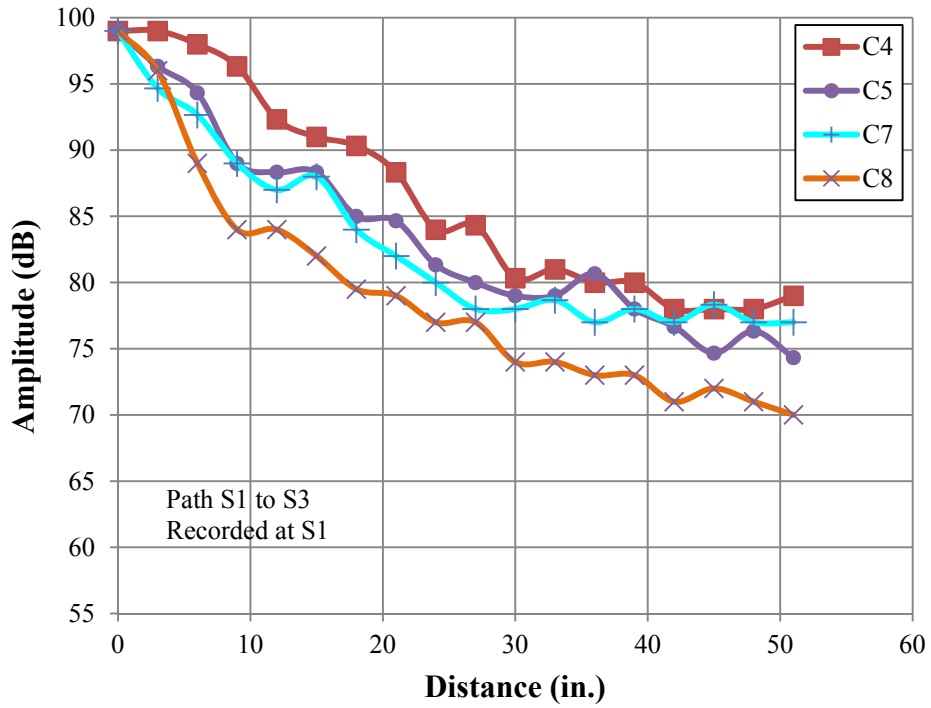

Fig. 3-6. Attenuation curves at 28 days for slabs C4, C5, C7 and C8. (Note: 1 in.=25.4 mm)

CHAPTER 4: STUDY 3 - EFFECTS OF CRACKS ON ACOUSTIC EMISSION WAVE PROPAGATION IN CONCRETE SLABS

SUMMARY

Various non-destructive testing techniques are now available for Structural Health Monitoring (SHM) and Acoustic Emission (AE) is one of them. A potential advantage of the AE technique is its capacity to locate active defects in Reinforced Concrete (RC) members if scattering and attenuation of stress waves can be successfully addressed. Due to the inhomogeneous nature of RC and presence of cracks, it is difficult to identify and characterize AE sources and their locations. This research experimentally studies the effects of cracks on AE wave propagation. Two similar RC slabs are manufactured and load tested. In parallel with the well-established measurements of load and strain, an active AE test is carried out throughout the load test. The results show that cracks can prominently affect the attenuation and velocity of AE waves. The outcome of this research can be used as a template and part of a database for AE wave attenuation and velocity in cracked RC members applicable in the field for SHM of concrete members.

BACKGROUND

The Acoustic Emission (AE) technique plays a progressively significant role in the field of non-destructive testing (NDT) especially in structural health monitoring (SHM). For AE to be a practical method to locate and assess damage and cracks in RC members, a clear and practical understanding of the attenuation and velocity of the acoustic waves in both cracked and un-cracked situations is essential. In this study, an attempt has been made to understand the changes in characteristics of AE waves while passing through a

cracked RC member. To meet this objective, two RC slabs are manufactured and loaded in a four-point bending setup. The loading pattern is designed to take into account loading and unloading stages in order to investigate both open and closed crack situations. At each step of loading, AE signals are generated at known locations using Pencil Lead Breaks (PLBs), an ASTM standard method (ASTM E1316 2010), and recorded by AE sensors at known locations. Effects of cracking parameters including maximum crack width, number of cracks and maximum crack depth are discussed and crack to slab depth ratio is chosen for correlation with AE wave attenuation and velocity. The results obtained from this study are utilized to provide information on wave attenuation and velocity in cracked RC members in the form of reference tables which can be applicable for AE in-situ tests and SHM purposes. These results complement the AE database for un-cracked concrete slabs previously proposed in study 2.

4.1 ACOUSTIC EMISSION OVERVIEW

AE terminology used in this study is briefly defined in this section. AE is a phenomenon of transient stress waves resulting from a sudden release of elastic energy caused by mechanical deformations, initiation and propagation of microcracks, dislocation movement and other irreversible changes in material (ASTM E1316 2010). These waves can be detected on the surface of specimens or structures by piezoelectric transducers which convert the mechanical vibrations to electric signals (AE signals). A signal that exceeds a defined threshold is called a "*hit*" and exceeding the defined threshold triggers the accumulation of data. If the same signal is recorded by more than one sensor, it is considered to be illustrative of a significant incident and is called an "*event*". Events can be recorded and analyzed to obtain further information regarding the source of the signals

(Carpinteri et al. 2008). To locate the source of these events, knowledge of wave propagation characteristics between source and receiver is necessary. Two fundamental concepts of AE wave propagation which are investigated in this study are "*wave attenuation*" and "*velocity*".

4.1.1 Wave Attenuation

Attenuation dampens a stress wave as the wave front propagates away from its source and spreads over a larger volume. Attenuation of a stress wave in an infinite medium causes the wave amplitude to decrease proportionally to the distance from the wave source (Miller and McIntire, 1987). RC has unique attenuation characteristics due to heterogeneity, porosity, presence of cracks and steel reinforcement. Besides internal damping, AE waves travelling in RC members undergo reflection, scattering, mode conversion and diffraction, all of which influence the propagation of stress waves (Miller and McIntire, 1987 and Al-Wardany et al. 2007). Wave attenuation limits sensor distance, which, in turn, limits the area that can be accurately monitored by a fixed number of sensors (Guratzsch and Mahadevan 2010). Therefore, attenuation is considered as having a major influence on the accuracy of data collected from RC members.

4.1.2 Wave Velocity

Knowledge of wave velocity is critical for AE source location. The most commonly used AE location method is known as the Time of Arrival (TOA) method, where the location of the damage can be determined from the TOA of the event at two or more sensors (Salinas et al. 2010). When using TOA method, the velocity of the wave that propagates

through the material needs to be known. An inaccurate assumption of wave velocity can contribute to large errors in source location (Muhamad Bunnori et al. 2006). Homogenous materials have well defined velocities, but this is not the case for inhomogeneous materials with possible cracks interfering with the AE wave propagation. The basis for the wave velocity calculation is the time-distance relationship implied by the velocity of the wave. The absolute arrival time, t, of a hit in an event can be combined with the velocity of the AE wave, v, to yield the distance, d, from the sensor to the source:

$$d = vt \tag{4-1}$$

In this equation, the distance d_i between the source of AE wave coordinates (x_0, y_0, z_0) and sensor i with known coordinates (x_i, y_i, z_i) can be found as:

$$d_i = \sqrt{(x_i - x_0)^2 + (y_i - y_0)^2 + (z_i - z_0)^2} \tag{4-2}$$

The distance of the source to the sensor "i" can also be given by:

$$d_i = v(t_i - t_0) \tag{4-3}$$

Where t_i is the TOA to the sensor i and t_0 is the time of event occurrence.

If the coordinates (x_0, y_0, z_0) of the AE source are known, by measuring TOA of the AE wave, the wave velocity can be calculated (Salinas et al. 2010).

4.2 EXPERIMENTAL PROCEDURE

4.2.1 Geometries and Material

Two RC slabs are manufactured and loaded in a four-point bending setup. **Fig. 4-1** shows the specimen, and loading frame setup. Each slab is instrumented with a total number of

four strain gages. Two are attached to two steel bars and the other two are located at the center of the top face of the slab (**Fig. 4-2**). The relevant geometry and material properties of the RC slabs are given in **Table 4-1**. As shown, three #3 steel bars are used as reinforcement. The geometry of the specimen and strength of the materials were selected so that the slab would be under-reinforced and display a ductile behavior with yielding of the steel preceding crushing of concrete. Based on conventional RC theory and nominal material properties as listed, the ultimate capacity of the slab would be reached at a moment value of 79,999 lb.in. (9.03 KN.m) corresponding to a load of 4,232 lb (18.8 KN) per loading point. Since the nominal sheer capacity is 6,329 lb (28.1 KN), flexural failure is expected. The concrete mixture design for both slabs is shown in **Table 4-2**. The compressive strength of concrete used for the slabs is measured by testing three 8 x 4 in. (203 x 102 mm) cylinders at 3, 7 and 28 days of age according to ASTM C39 specifications (ASTM C39 2010). The compressive strength of 3050 psi (21.0 MPa) is reached after 28 days of curing as an average of three compression tests with coefficient of variation of 0.02. The yield strength of steel bars as per manufacture's mill certificate is 60,000 psi (414 MPa). The slabs are whitewashed using lime wash to enhance the visibility of cracks and facilitate their measurements.

4.2.2 AE Equipment and Setup

The PAC Sensor Highway II system (AEwin Software User's Manual 2009) equipped with R6I-AST resonance sensors is used for AE data collection. This system with 16 high-speed AE channels is designed for unattended and remote monitoring use, and includes AEWin software (AEwin Software User's Manual 2009) for data analysis. The R6I-AST resonance sensors have an operating frequency range of 40 - 100 kHz and a

resonant frequency of 55 kHz. The maximum detectable amplitude for R6I sensors is 100 dB, corresponding to the amplitude of the amplified signal when it reaches 10 volts (saturation limit of the system). To ensure proper coupling of each AE sensor, a two-part epoxy contact agent is applied to connect the sensors to the concrete surface.

The acquisition parameters in the AEWin software are summarized in **Table 4-3**. A detailed explanation of these parameters is offered in (AEwin Software User's Manual 2009) and is outside the scope of this study. **Table 4-3** is provided here so that other researchers can repeat this experiment. The level of the environmental noise amplitude is measured by acquiring AE data for one hour while the hydraulic pump is running and the actuator is applying 700 lb (3115 N) to the slab. As a result, a maximum noise level of 35 dB is determined and this amplitude level is used as the recording threshold for relevant AE waves.

All sixteen available channels are used to record the signals originating from 16 sensors attached to each slab. The sensor configuration is shown in **Fig. 4-2**. To eliminate the non-relevant signals coming from the loading points and the supports, six sensors at the top (S_{11} to S_{16}), four sensors on the sides (S_7 to S_{10}) and two sensors at bottom (S_1 and S_6) faces of each slab are used as guard sensors (**Fig. 4-2**). This is a noise rejection technique based on wave arrival times: if an AE wave is detected first by a guard sensor, it is ignored in the analysis because the source of the wave is assumed to be outside the area of interest. The four main sensors (i.e., sensors S_2 to S_5) all applied to the bottom face of the slab are assigned to the zone of interest where crack formation is predicted (**Fig. 4-2**). This sensor positioning in a linear configuration allows investigating the effects of newly formed cracks at each step of loading and creates a simplified 2D environment in which

the cracks surface is perpendicular to the sensor line. A similar situation can be replicated in real applications in the case of one-way flexural members.

4.3 LOADING PROCEDURE AND AE TEST

The load test is conducted according to a loading protocol consisting of 10 steps (**Fig. 4-3**). These steps are designed to allow for AE parameters to be investigated before and after critical points such as concrete cracking and reinforcement yielding.

The AE test is performed by PLBs at given locations on the bottom of each slab to generate acoustic waves while the sensors are acquiring AE data. This PLB test starts at step 1 and is repeated after each step of loading and unloading while the load is kept constant for an average of 5 minutes (steps 2 to 10). At each PLB test all sensors are recording. Only the data recorded by main sensors (i.e., sensors S_2 to S_5) are utilized for attenuation and velocity calculation. The other sensors (guard sensors) are employed to eliminate all signals other than PLB signals. In **Fig. 4-2**, the "X"s on the bottom centerline of the slabs represent the locations at which PLBs are performed. In order to minimize and uniformly distribute the operator errors, the PLBs are repeated three times at each position following a fully randomized order. The purpose of unloading and performing PLB tests after each load cycle is to determine AE wave characteristics when the cracks are closed.

4.4 DISCUSSION AND RESULTS

The concrete cracking and yield points observed in the experiments closely matched the analytically predicted values. The data from strain gages is utilized to identify the reinforcement yield point and the depth of neutral axis at each load level.

The visible cracks are marked, measured and photographed for further post-test analysis, while the load is constant in each loading step. **Fig. 4-4**, as an example, shows the geometry and configuration of cracks for both slabs at step 5 of loading described in **Fig. 4-3**. In the two pictures, crack lines are manually accentuated on visible cracks for purpose of clarity. At each step of loading, maximum crack width, number of cracks and maximum crack depth are determined and measured. The two slabs have almost identical behavior. The observations from two slabs are summarized in **Table 4-4**. In this table, step numbers and their respective descriptions are shown in the first two columns. Applied load at each step and the corresponding maximum moment are presented in the columns 3 and 4. Maximum crack width and number of cracks in the central 36 in. section based on visual measurement are reported in columns 5 and 6. Average strain readings on reinforcements and concrete extreme fiber are shown in column 7 and the values are used to calculate the crack depth based on the position of the neutral axis. Visual crack depth is presented along with the calculated crack depth in column 8.

4.4.1 Attenuation

AE waves resulting from PLBs are recorded by four main sensors (S_2 to S_5). Attenuation at 9, 18, 27 and 36 in. 9 (0.22, 0.45, 0.68 and 0.91 m) are measured by calculating the loss of amplitude of a wave traveling between the source (PLB) and the selected sensor. The paths between PLBs and the main sensors chosen for attenuation analysis are presented in **Table 4-5**. Attenuation values are calculated using the average of all PLBs performed for a given distance using the sensors indicated in the table.

Fig. 4-5 shows the attenuation curves in the format of attenuation vs. applied moment for two slabs and for above-mentioned distances while slabs are loaded and cracks are open.

In these graphs, the drop of amplitude at a certain distance from the recording sensor represents the attenuation over that distance. Attenuation limits maximum sensor distance, which, consequently, limits the area that can be accurately monitored by a fixed number of sensors. As expected, by increasing the moment and initiation of new cracks or propagation of existing cracks attenuation increases. This means that an AE sensor in a cracked media can cover a significantly smaller area compared to the area that it can cover in an un-cracked media. For example, if the goal is to elect concrete cracks with source amplitude over 60 dB and the recording threshold level to exclude environmental noise is 40 dB, in un-cracked situation the 18 in. (0.45 m) distance from source to sensor is sufficient, but the maximum covered distance in the cracked case is 9 in. (0.22 m).

A sharp jump in attenuation is seen after first concrete cracking (**Fig. 4-5**). With propagation of cracks and formation of new cracks, attenuation increases in an almost linear fashion. A similar trend is seen for all four chosen distances. Thus, the existence of cracks introduces additional attenuation and this influences the accuracy of data collected from RC members and should be considered prior to deciding the sensor arrangement.

As an example, **Fig. 4-6 a** and **b** show the wave attenuation for the two slabs at 9 and 36 in. (0.22 and 0.91 m) in different steps of loading for both open crack (loaded) and closed crack (unloaded) situations. These two distances have been chosen as they represent the two extreme cases in this project. The X-axis in these two figures shows the maximum "experienced" moment of the member at each step thus the vertical lines represent both loading and unloading steps. This means that in the unloading stage, the maximum experienced moment remains constant as the load is decreased. It is observed that crack closure has little impact on AE signal attenuation. This shows that closed cracks while

member is unloaded, can affect signal attenuation almost as severely as open cracks under loads.

A reference table (**Table 4-6**) for AE monitoring of RC slabs, which can provide guidance about the member's attenuation was previously developed in study 2. The results from the attenuation tests provided in this study are utilized to develop a supplementary table that can provide further guidance about attenuation in the presence of cracks for RC slabs with similar characteristics. This supplementary table has the potential to be expanded to cover various slab properties and cracking patterns. In order to choose a relevant crack parameter which has the most effect on signal attenuation and can be employed in the supplementary reference table various parameters including maximum crack width, number of cracks and maximum crack depth are considered.

- Crack Width

Crack width is a function of the applied load, geometry and load history of the member. As seen in **Fig. 4-6** crack closure has less than 7% effect on AE signal attenuation. If a cracked slab has experienced higher load levels, the crack width at a given time is not representative of the severity of the damage given that crack closure exists. As a result, crack width is not considered as a parameter effecting AE attenuation in concrete slabs.

- Number of Cracks

In order to investigate the effect of number of cracks on wave attenuation, the zones between sensors S_2 - S_3 and sensors S_4 - S_5 in slab S1 are monitored in step 7 as they include different numbers of cracks yet have the same sensor distances (**Fig. 4-7**). The zone between sensors S_4 and S_5 contains two cracks (a and b) while the zone between sensors S_2 and S_3 includes one crack (c). All three cracks have similar depths (**Fig. 4-7**).

The signals generated by PLBs beside sensors S_2, S_3, S_4 and S_5 in step 7 are used for this assessment. PLBs performed by S_4 and recorded by S_5 and vice versa show an average of 45 dB/9 in. (45 dB/23 cm) attenuation and PLBs performed by S_2 and recorded by S_3 and vice versa show an average of 44 dB/9 in. (44 dB/23 cm) attenuation. As drop in amplitude is very close for these two cases with different number of cracks, it is concluded that the "number of cracks" cannot be seen as an influential parameter on attenuation of AE waves. Whereas this is the case for the two slabs tested, the number of cracks could impact attenuation in other cases particularly if the distance between source and receiver were to be longer or if the cracks were to form with directions not perpendicular to the line connecting source and receiver.

- Crack Depth

Crack depth is expected to have an effect on the wave propagation as with crack propagation, the cross sectional area from which the wave is transmitted is lost. In order to verify the effect of crack depth, the zone between sensor S_2 and S_3 in slab S1 is monitored as it included only one crack (c) during the steps 3, 5 and 7 of the test. PLBs performed at these steps beside sensor S_2 and S_3 are used for the analysis. PLBs performed by S_2 and recorded by S_3 and vice versa show an average of 27 dB/9 in. (27 dB/23 cm), 36 dB/9 in. (36 dB/23 cm) and 44 dB/9 in. (44 dB/23 cm) attenuation in steps 3, 5 and 7. As a result, it is concluded that the crack depth has a prominent effect on signal attenuation.

As a unit-less parameter, crack to slab depth ratio (R_c) is chosen to correlate the effect of cracking with changes in signal attenuation of the acoustic wave. The average maximum crack depth and accordingly R_c for loading steps 3, 5, 7 and 9 is calculated using values

from column 8 of **Table 4-4**. In order to calculate the "extra" attenuation corresponding to the R_c values, the expected attenuation for un-cracked member (**Table 4-6**) and the calculated attenuation at each loading step are shown in **Table 4-7**. In this table the first column shows the selected attenuation distances. The expected attenuation for un-cracked RC slabs are calculated by interpolation from **Table 4-6** and presented in the second column. The calculated attenuation at loading steps 3, 5, 7 and 9 are shown in the third column. Extra attenuation due to cracking are computed by subtracting the values of column 2 from column 3 and presented in the fourth column.

As a result, **Table 4-8** can be generated relating "extra" attenuation (that is attenuation due to cracking) to the crack to slab depth ratio (R_c). In case of AE monitoring of cracked slabs, these values need to be added to the values presented in **Table 4-6**. Companion **Tables 4-6** and **4-8** are only applicable for slabs with spelled out characteristics and R6I sensors. Existing AE sensors offer a variety of different features (e.g. preamplifiers, internal filters, power required and gain) that make them suitable for various purposes. As different types of sensors perform differently, it is necessary to include the sensor type in any database. **Tables 4-6** and **4-8** together can provide guidance about the member's attenuation in presence of cracks especially when sensor spacing and source location are concerned. For instance, expected attenuation in 20 in. (508 mm) for an un-cracked RC slab with normal weight/crushed aggregate is 21 dB (**Table 4-6**). If the same slab is cracked with R_c between 55% to 65%, based on **Table 4-8**, 21 dB attenuation should be added to the previous value and a total 42 dB attenuation in cracked situation should be expected.

4.4.2 Velocity

For both slabs the wave velocity is derived at all loading steps as illustrated in **Fig. 4-3**. All 15 PLBs performed at each step of the test are included to calculate the velocity of the AE waves for the given step. Since the basic velocity calculation is applied to a single signal (PLB), an optimization procedure to calculate wave velocity can be implemented. The procedure developed to calculate the optimal wave velocity through the slab under consideration consists of these steps:

a) Selecting the TOAs

b) Defining the overall error based on calculated and known locations of the PLBs

c) Minimizing the overall error

d) Finding the optimal velocity

The procedure is performed using AE data recorded by sensors S_2 and S_5. In step (a) TOAs of each PLB to the end sensors (S_2 and S_5) are selected automatically by AEWin software based on their waveforms. The automatic determination of TOA is based on a threshold (in dB scale). TOA is calculated from the first signal excursion above the threshold. In this procedure, three threshold levels (30, 35 and 40 dB) are considered to determine the TOA for each signal.

For each PLB located between two sensors, d_2 and d_1 are the calculated distances of PLB $_j$ to the end sensors and D_2 and D_1 are the exact distances. In steps (b) and (c), the optimal velocity is defined so that the overall error, E_D, between the difference of calculated distances $\Delta d_j = (d_2 - d_1)_j$ of PLB $_j$ to the end sensors and their actual values, $\Delta D_j = (D_2 - D_1)_j$, is minimized. Defining the error as:

$$E_D^2 = \sum_{j=1}^{n} \left(\Delta D_j - \Delta d_j\right)^2 = \sum_{j=1}^{n} \left(\Delta D_j - v\Delta t_j\right)^2 \quad (4\text{-}4)$$

Where $\Delta t_j = (t_2 - t_1)_j$ and the automatically recorded arrival times of PLB $_j$ to the end sensors are t_1 and t_2 .The overall error can be minimized by:

$$\frac{\partial E_D^2}{\partial v} = 0 \rightarrow \sum_{j=1}^{n} \Delta t_j \left(\Delta D_j - v \Delta t_j\right) = 0 \tag{4-5}$$

Resulting in the optimal velocity, v of:

$$v = \frac{\sum_{j=1}^{n} \Delta t_j \Delta D_j}{\sum_{j=1}^{n} \Delta t_j^{\,2}} \tag{4-6}$$

In step (d), by substituting all TOAs selected in step (a) and known location of PLBs in Eq. (4-6) the optimal velocity is calculated.

Fig. 4-8 a and **b** show calculated velocities in different steps of loading considering three threshold levels (30, 35 and 40 dB) for both slabs. In this figure, at each step of loading the calculated velocity is a single value for path between sensors S_2 and S_5 and is not affected by the distance between source and receiver. It is observed that wave velocity is dependent upon the threshold level, higher threshold levels prolong the TOA of the wave and the velocity is reduced. This conversely, a significant drop in wave velocity is seen after the concrete cracking point and it can be observed that wave velocity is highly dependent on the presence of cracks it further decreases with the progress of the test.

In order to investigate the effect of crack closure on wave velocity, in each loading and unloading step wave velocity is calculated and presented in **Fig. 4-9 a** and **b**. For brevity, only the results obtained for threshold of 35 dB are displayed. Similarly to **Fig. 4-6**, the X-axis in these figures shows the maximum experienced moment of the member at each step thus the vertical lines represent both loading and unloading steps. It is observed that closed cracks affect AE wave velocity as severely as open cracks. Similar trends are found for all threshold levels.

Table 4-9 shows wave velocity for un-cracked RC slabs at values of the selected threshold levels (study 2). The velocity results obtained from this study are utilized to develop a supplementary table that accounts for the presence of cracks. In order to choose a relevant crack parameter to be used in the supplementary reference table, similar to what was done for attenuation, maximum crack width, number of cracks and crack depth are studied.

- Crack Width

As shown in **Fig. 4-9**, closed cracks can affect AE wave velocity almost as severely as open cracks as less than 5% change is seen in velocity values for different loading steps in the two cases. Thus, in this study crack width is not considered an influential parameter on wave velocity.

- Number of Cracks

In order to investigate the effect of number of cracks, the zones between sensors S_2 - S_3 and sensors S_4 - S_5 in slab S1 which was investigated for attenuation are examined (**Fig. 4-7**). PLBs performed by S_4 and S_5 and recorded by S_2 and S_3 in step 7 are substituted in the velocity algorithm. The velocity between sensors S_4 - S_5 containing two cracks (cracks a and b in **Fig. 4-7**) and S_2 and S_3 containing only one crack (crack c in **Fig. 4-7**) are calculated and shown in **Table 4-10** for three different threshold levels. As the difference between the calculated velocities for the two cases with different numbers of cracks is less than 3.5%, it is concluded that the number of cracks does not have a major effect on AE wave velocity.

- Crack Depth

In order to investigate the effect of crack depth on wave velocity the zone between sensor S_2 and S_3 in slab S1 is monitored. Calculated velocities for three threshold levels in steps 3, 5 and 7 are presented in **Table 4-10**. As shown, velocity is significantly different for these steps while only one crack existed in the wave path. Based on these observations, it is concluded that crack depth has a prominent effect on velocity of AE wave. Thus, the same parameter (R_c) used for attenuation is chosen to describe the nature of the cracked media to be correlated with changes in velocity of the acoustic wave.

R_c values previously calculated for loading steps 3, 5, 7 and 9 are applied. In order to calculate the drop in velocity and relate it to corresponding R_c value, the expected velocity for un-cracked member captured from **Table 4-6** and the calculated velocity at loading steps are compared in **Table 4-11**. In this table the first column shows the three threshold levels for which the velocities are calculated. The expected AE wave velocities for un-cracked RC slabs are presented in the second column. The calculated velocity at loading steps 3, 5, 7 and 9 are shown in the third column. By comparing the calculated velocities and the expected velocity values, drop in velocity is calculated and presented in the fourth column. As shown in **Table 4-11**, threshold level has little effect on drop of velocity since drops in velocities are similar for three threshold levels. By using the average velocity drop at each step of loading and respected R_c, a template for drop of velocity due to cracking is developed (**Table 4-12**). In presence of cracks, values presented in this table need to be subtracted from the values given in **Table 4-9**. As per attenuation table, this table is only applicable for slabs with spelled out characteristics and R6I sensors. It should be noted that this supplementary table is formed based on limited number of tests and only presents a data point that can be expanded to cover a

broader range of slabs and crack attributes. In the following section with an example, the importance of using variable velocity in presence of cracks for source location is demonstrated.

4.4.3 AE source location using variable velocity

As seen above, in the presence of cracks wave velocity decreases during the load test. Thus, accuracy of AE source location at all stages of the test can be maintained and improved by introducing "variable" velocity. In other words, for crack location at each step of loading a new velocity calculated from previous step can be applied.

Improvement of location results in study 3: To demonstrate this improvement, slab S1 is used as an example. In this test while loading from steps 4 to 5, a single crack (d) appears between sensors S_3 and S_4 while other existing cracks only marginally extend (**Fig. 4-10 a**). First, using the wave velocity related to un-cracked case (**Table 4-9**) and AEwin point location built-in algorithm, the crack (d) location is determined. Then, the same procedure is repeated and crack (d) location is calculated using the new velocity calculated after step 3 (**Table 4-9** and **Table 4-12**). The overlay of the visual crack (d) versus calculated crack (d) using the two velocity values is shown in **Fig. 4-10 a** and **b**. In the underlying graph, cumulative numbers of events generating from crack (d) (Y-axis) versus crack (d) location (X-axis) are presented. Since only the crack (d) is concerned, other cracks are not shown in these graphs. As the location of the visual crack (d) is known, the change in accuracy of AE location results can highlight the effect of the "variable" wave velocity on source location. As is seen, the error in location is approximately 3 in. (76 mm) in case the effects of cracked media are ignored. Using the variable velocity, the error is decreased to approximately 1.5 in. (38 mm). The 50%

improvement caused by implementing variable velocity in source location in cracked concrete slabs can be clearly seen in this case.

Improvement of location results in study 1: To investigate the importance of study 3 and the effectiveness of using "variable" velocity for AE source location in cracked media, the "variable" wave velocity is used to locate the cracks for load test performed in study 1. The goal is to compare the location of cracks captured in study 1 using constant velocity versus "variable" velocity. For clarity only one crack that became visible between load levels of 5000 to 6000 lb (22.2 to 26.6 kN) is used for this purpose (**Fig. 4-11**). **Fig. 4-11 a** shows the crack which is located with constant velocity of 120,000 in/s (3048 m/s) captured during pre-test (study 1) and **Fig. 4-11 b** shows the crack which is located with velocity captured from **Table 4-12** (study 3). In order to use **Table 4-12** the value of R_c is needed. Considering cross section and geometry shown in **Fig. 2-1** and 5000 lb (22.2 kN) applied load, crack depth of 2.68 in. (68 mm) is expected. The R_c thus is equal to 0.53. **Table 4-12** is used to estimate the wave velocity for the calculated R_c. The wave velocity is calculated to be equal to 75000 in/s (1778 m/s) and the value is used as input velocity in location procedure (**Fig. 4-11**). It is observed that the location of crack is marginally better estimated and less scattered using "variable" velocity. It needs to be noted that limited number of sensors are available and errors in location technique can be minimized if more sensors are used.

4.5 CONCLUSIONS

In order to identify the influence of concrete cracking on both signal attenuation and wave velocity two RC slabs are load tested and the effects of cracking parameters

including maximum crack width, number of cracks and maximum crack depth are discussed. The following observations are made:

1. In the presence of cracks, attenuation increases and wave velocity decreases.
2. Closed cracks affect signal attenuation and wave velocity almost as severely as open cracks under loading.
3. Among crack parameters, crack depth has the most influence on wave attenuation and velocity.
4. Velocity is dependent upon the threshold level, higher threshold levels prolong the TOA of the wave and the velocity is reduced.
5. Threshold level has little effect on drop of wave velocity due to cracking.
6. Using "variable" velocity can improve AE source location in presence of cracks considerably.

Based on observation captured during this study, R_c value is chosen to represent the severity of cracking and other parameters for this purpose can be introduced and utilized. The results are utilized to provide information on wave attenuation and velocity in cracked RC members in form of tables which can be part of a reference database applicable for AE in-situ tests and SHM purposes. These results can be added to the database for un-cracked concrete slabs formerly introduced in study 2 especially valuable when source location is concerned. Different parameters representing the cases observed in the field (as boundary conditions, geometry, crack patterns, etc.) can be included and possible effects of them on attenuation and velocity of AE waves need to be investigated. It also needs to be noted that the suggested attenuation and velocity values are given for R6-I sensors and different sensors behave differently.

The attenuation and velocity results are calculated based on averaging and error minimization techniques for two tested slabs with a certain reinforcement, aggregate type and geometry. Thus, the results of this study cannot be applicable in all cases and a more comprehensive test matrix is required to cover wider range of slabs that exist in the field.

Table 4-1: Summary of as-built RC slab properties

Span	5 ft (1.83 m)
Shear Span	21 in. (533 mm)
Thickness	6.0 in. (152 mm)
Effective reinforcement depth	4.8 in. (122 mm)
Width	12 in. (305 mm)
Nominal concrete strength	3,000 psi (21 MPa)
Nominal steel strength	60,000 psi (414 MPa)
Main reinforcement	#3@4 in. (9.5@102 mm)

Table 4-2: Concrete mixture constituents

Slab	Coarse aggregate (lb/yd^3)	Fine aggregate (lb/yd^3)	Cement (lb/yd^3)	Water reducer (oz/yd^3)	Water (lb/yd^3)	Slump (in.)	W/C
C1-C2	818	2,103	571	35	314	5	0.54

1 lb/yd^3 = 0.59 Kg/m^3, 1 in. = 25.4 mm, 1 oz/yd^3 = 0.037 Kg/m^3

Table 4-3: Summary of layout selected in AE data acquisition software

parameters		Units	Value
Threshold		[dB]	35
Analog Filter	Lower	[kHz]	40
	Upper	[kHz]	100
Waveform Setup	Sample Rate	[MSPS]	1
	Pre-Trigger	[µs]	200
	Length	[points]	1024
Timing Parameters	PDT*	[µs]	300
	HDT**	[µs]	500
	HLT***	[µs]	100
	Max Duration	[µs]	99

* Peak Definition Time
** Hit Definition Time
*** Hit lockout Time

Table 4-4: Loading steps and experimental observations for slabs S1 and S2

Feature (1)	**Step # *** (2)	**Total applied load (lb)** (3)	**Maximum applied moment (lb.in.)** (4)	**Maximum crack width (in.)** (5)		**# of cracks in central 36 in. wide zone** (6)		**Average of strain gage readings (μs)** (7)				**Maximum crack depth (in.)** (8)			
								Concrete	Rebar	Concrete	Rebar	Visual	From Strains	Visual	From Strains
				S1	S2	S1	S2	S1		S2		S1		S2	
No load	1	0	0	0	0	0	0	0	0	0	0	0	0	0	0
Pre cracking	2	2,000	21,000	0	0	0	0	120	120	140	110	0	0	0	0
Cracking**		**3,000**	**31,500**												
Post cracking	3	3,100	32,550	0.005	0.005	3	3	980	580	840	650	3.3	3.0	3.5	3.3
	4	1,000	10,500	-	-	-	-	-	-	-	-	-	-	-	-
Intermediate	5	5,000	52,500	0.007	0.008	6	6	740	1180	710	1320	3.75	4.2	3.9	4.3
	6	1,000	10,500	-	-	-	-	-	-	-	-	-	-	-	-
Pre yield	7	7,800	81,900	0.015	0.01	8	9	990	2300	920	2510	4.5	4.6	4.6	4.7
	8	1,000	10,500	-	-	-	-	-	-	-	-	-	-	-	-
Yield***		**8,200**	**86,100**												
Post Yield	9	8,600	90,300	0.025	0.025	11	10	2640	-	2370	-	4.9	-	5	-
	10	1,000	10,500	-	-	-	-	-	-	-	-	-	-	-	-

1 lb = 4.45 N, 1 in. = 0.0254 m, 1 lb.in. = 0.113 N.m

* See Figure 4-3

**Analytical cracking load was 2,817 lb

***Analytical yield load was 8,465 lb

Table 4-5: PLB locations and chosen paths for attenuation

Distance (in.)	PLB location next to :	Recording Sensor
9	**Mid Span**	**S_3 and S_4**
18	S_3	S_4
	S_4	S_3
27	S_3	S_5
	S_5	S_3
36	S_2	S_5
	S_5	S_2

1 in. = 0.0254 m,

Table 4-6: Attenuation for un-cracked RC slabs (study 2)

Concrete type	Attenuation (dB)				
	Source distance (in.)				
	10	**20**	**30**	**40**	**50**
Normal-weight/Crushed aggregate	15	21	25	27	29

1 in. = 25.4 mm

Note:

Given values are independent of concrete compressive strength and maximum aggregate size and applicable to slabs with less than or equal 6 in. thickness.

Given values are for R6-I sensors.

Table 4-7: Attenuation at loading steps for slabs S1 and S2

	Distance (in.) (1)	**Un-cracked RC attenuation (dB)*** (2)	**Calculated attenuation (dB)** (3)				**Extra attenuation (dB)** (4)			
			step 3	step 5	step 7	step 9	step 3	step 5	step 7	step 9
Slab 1	9	14	28	35	44	51	14	21	30	37
	18	20	32	38	49	54	12	18	29	34
	27	24	38	45	56	60	14	21	32	36
	36	26	40	49	58	63	14	23	32	37
Slab 2	9	14	28	35	44	51	14	21	30	37
	18	20	32	38	49	54	12	18	29	34
	27	24	38	45	56	60	14	21	32	36
	36	26	40	49	58	63	14	23	32	37
Average							13.5	20.75	30.75	36

1 in. = 0.0254 m
* Reference study 2

Table 4-8: Extra attenuation for cracked RC slabs

Crack to slab depth ratio (%) (R_c)	Attenuation due to cracking (dB)
$R_c \leq 55$	14
$55 < R_c \leq 65$	21
$65 < R_c \leq 75$	31
$75 < R_c \leq 85$	36

1 in. = 0.0254 m,
Note: Given values are for slabs of Table 6 and R6-I sensors

Table 4-9: Velocity for un-cracked RC slabs (study 2)

Concrete compressive strength (psi)	Velocity (in/s x 10^5)		
	Threshold level (dB)		
	30	35	40
< 4000	1.27	1.22	1.14

1000 psi = 6.9 MPa, 1 in. = 25.4 mm
Note:
Given values are applicable to slabs with normal-weight concrete, crushed aggregate, ½ in. maximum aggregate size, less than or equal 6 in. thickness.
Given values are for R6-I sensors.

Table 4-10: Velocity at loading steps for limited sensors

Step #	Path	Velocity (in/s x 10^5)		
		Threshold level (dB)		
		30	35	40
3	S2-S3	0.84	0.79	0.73
5	S2-S3	0.68	0.63	0.58
7	S2-S3	0.43	0.39	0.36
	S4-S5	0.42	0.38	0.34

1 in. = 0.0254 m

Table 4-11: Velocity at loading steps for slabs S1 and S2

	Threshold (dB) (1)	Un-cracked RC Velocity (in/s x 10^5)* (2)	Recorded Velocity (in/s x 10^5) (3)				Drop of Velocity (in/s x 10^5) (4)			
			step 3	step 5	step 7	step 9	step 3	step 5	step 7	step 9
Slab 1	30	1.27	0.87	0.69	0.44	0.41	0.40	0.58	0.83	0.86
	35	1.22	0.82	0.65	0.41	0.36	0.40	0.57	0.81	0.86
	40	1.14	0.75	0.59	0.36	0.32	0.39	0.55	0.78	0.82
Slab 2	30	1.27	0.88	0.67	0.46	0.40	0.39	0.60	0.81	0.87
	35	1.22	0.84	0.62	0.42	0.34	0.38	0.60	0.80	0.88
	40	1.14	0.76	0.58	0.37	0.29	0.38	0.56	0.77	0.85
Average							0.40	0.57	0.82	0.86

1 in. = 0.0254 m

* Reference study 2

Table 4-12: Drop of velocity for cracked concrete slabs

Crack to slab depth ratio (%) (R_c)	**Velocity drop due to cracking (in/s x 10^5)**
$R_c \leq 55$	0.40
$55 < R_c \leq 65$	0.57
$65 < R_c \leq 75$	0.82
$75 < R_c \leq 85$	0.86

1 in. = 0.0254 m,
Note: Given values are for slabs of Table 6 and R6-I sensors

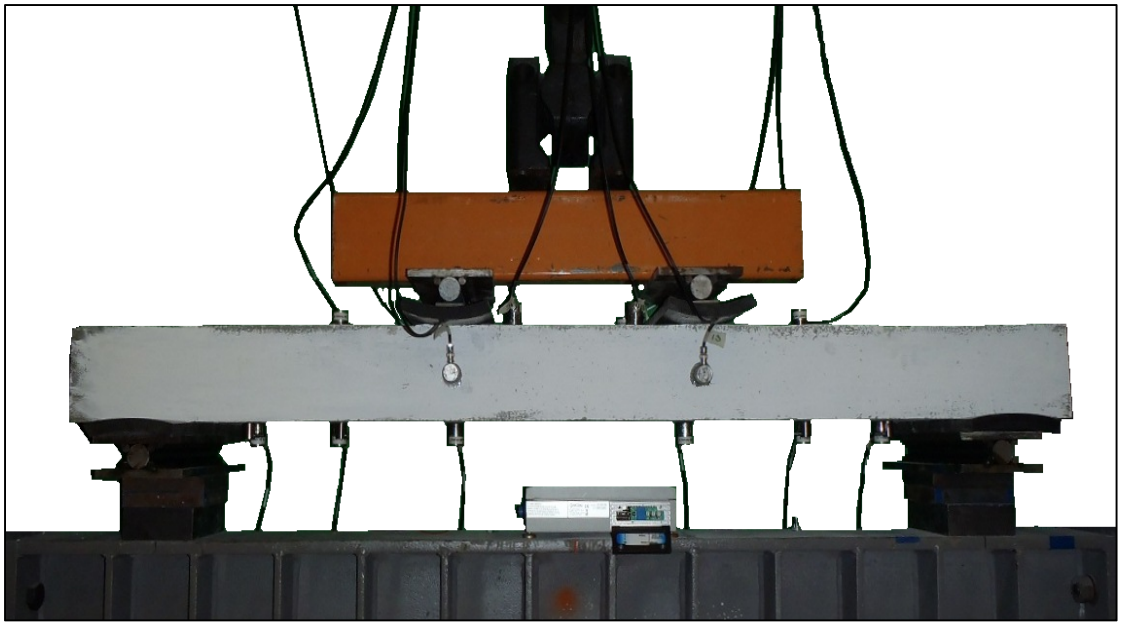

Fig. 4-1. Load test setup

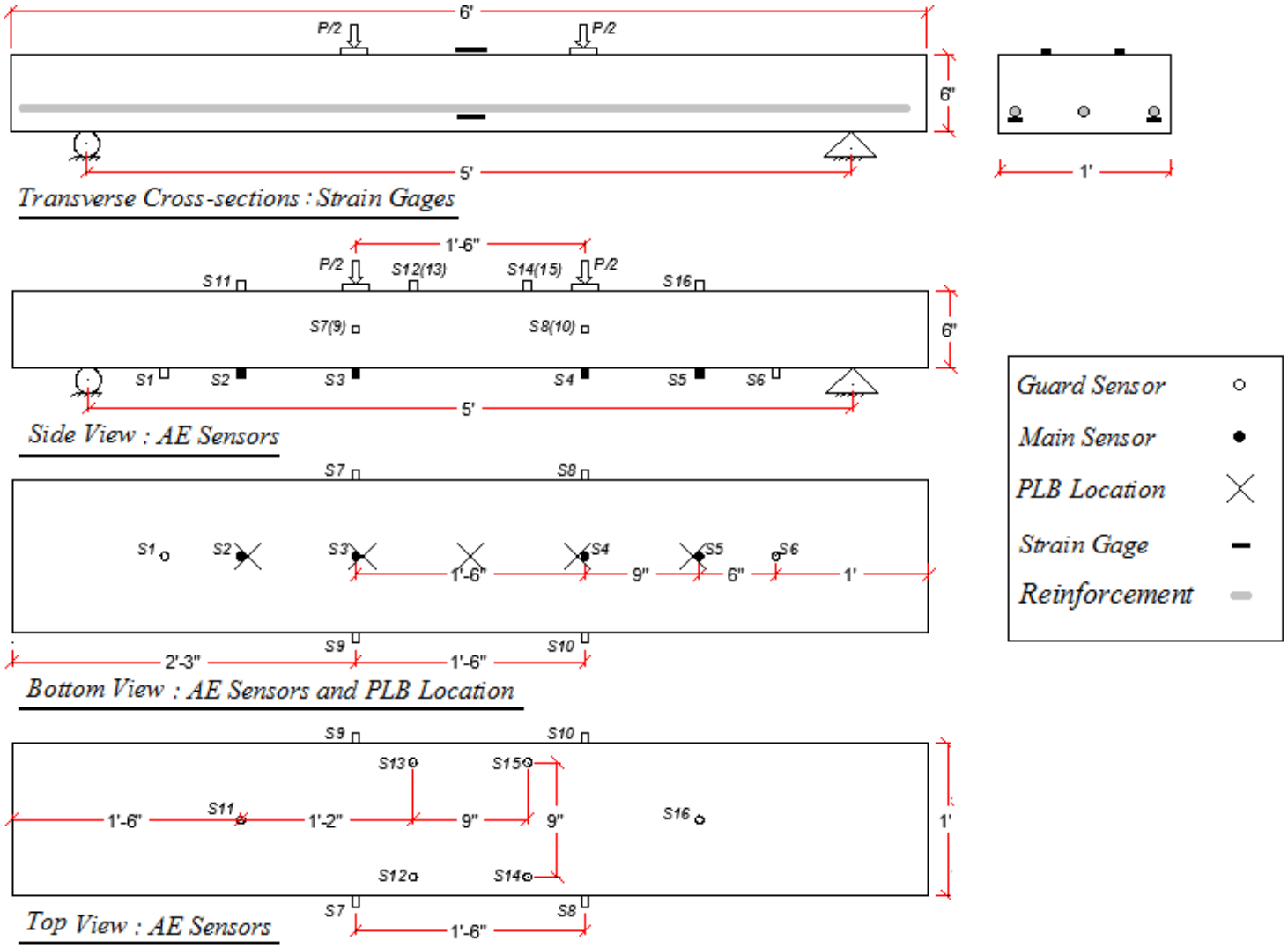

Fig. 4-2. Strain gages, AE Sensors and PLBs locations. (Note: 1 in.=25.4 mm)

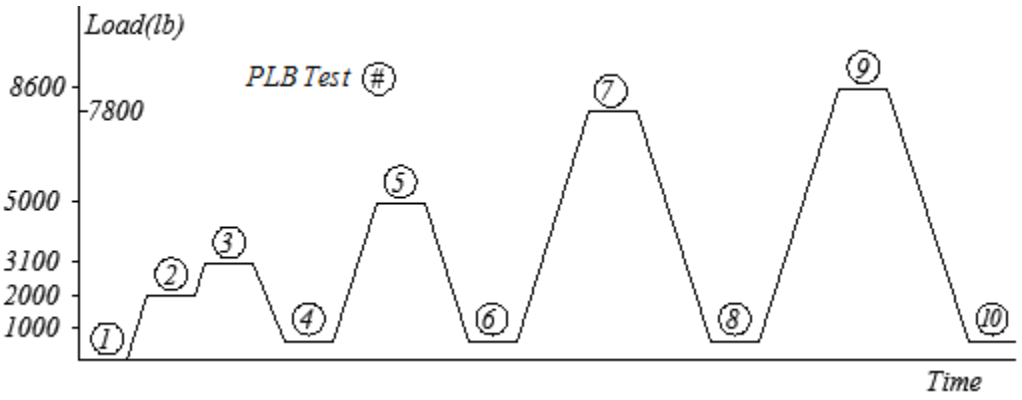

Fig. 4-3. Loading steps and AE tests performed. (Note: 1,000 lb=4.448 kN)

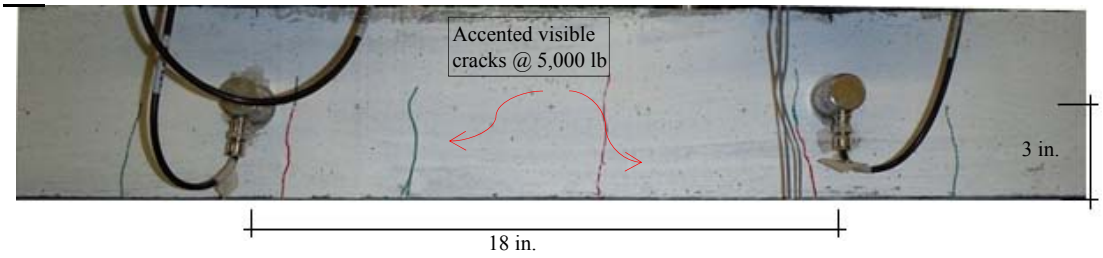

a)

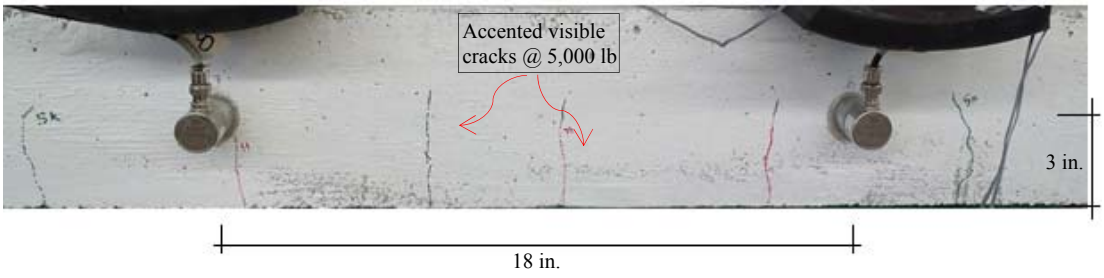

b)

Fig. 4-4. Visible cracks for load step 5: a) slab S1 b) slab S2

(Note: 1,000 lb=4.448 kN, 1in.=25.4 mm)

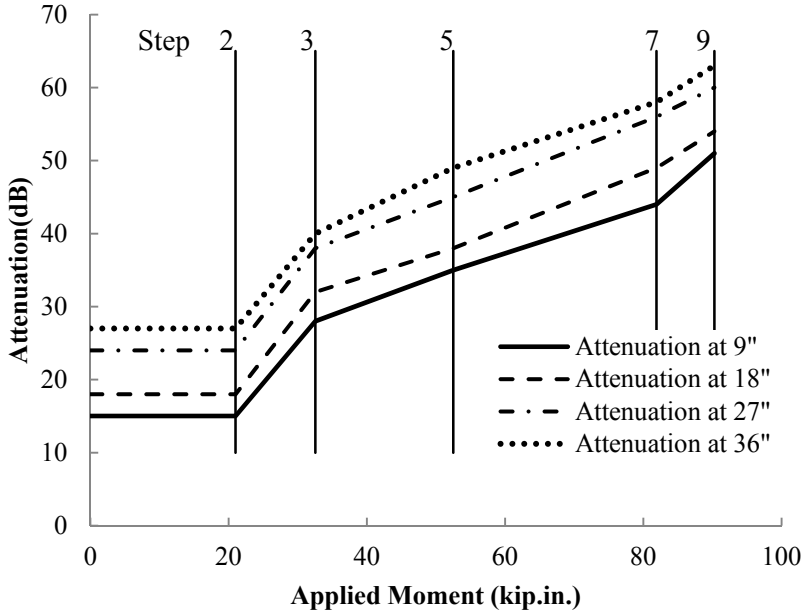

a)

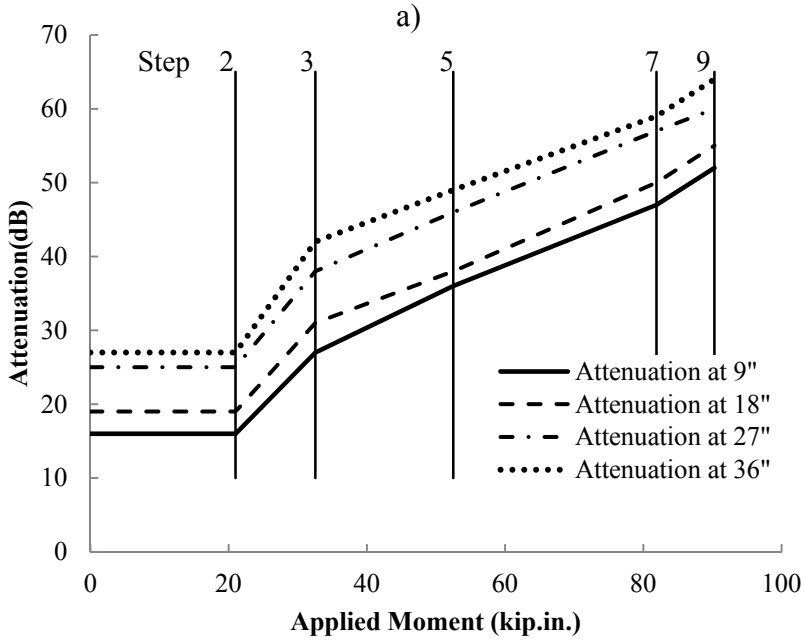

b)

Fig. 4-5. Attenuation at different load steps for various distances: a) Slab S1 b) Slab S2 (Note: 1 lb.in. = 0.113 N.m, 1in.=25.4 mm)

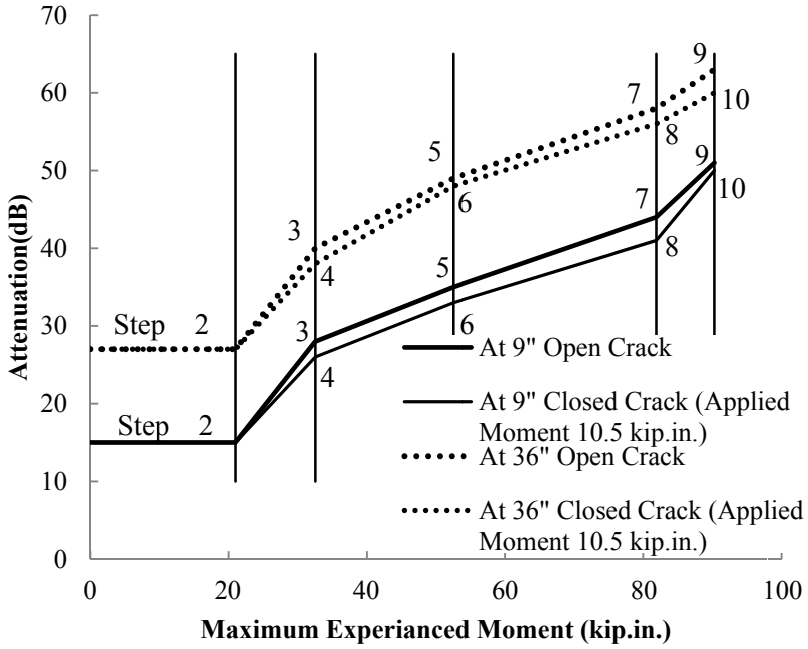

a)

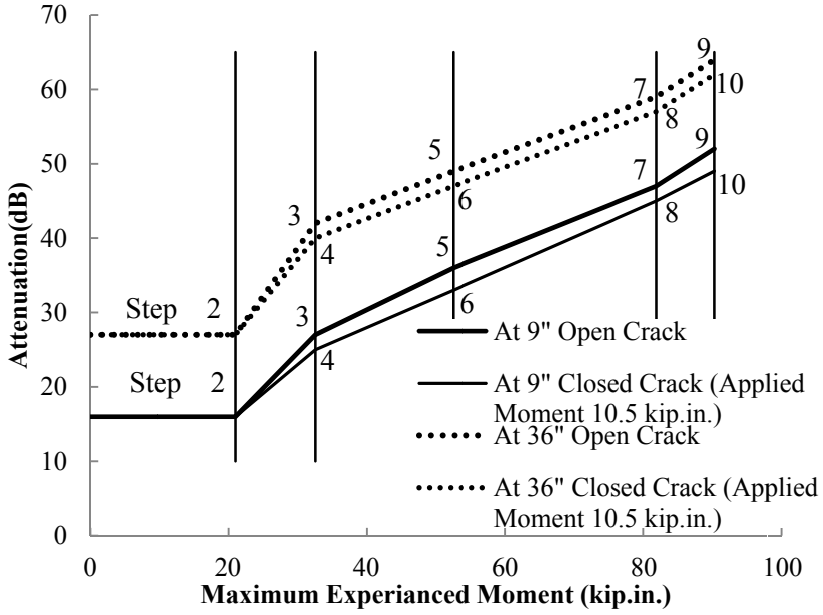

b)

Fig. 4-6. Attenuation for different load steps at 9 and 36 in. distances: a) Slab S1 b) Slab S2 (Note: 1 lb.in. = 0.113 N.m, 1in. =25.4 mm)

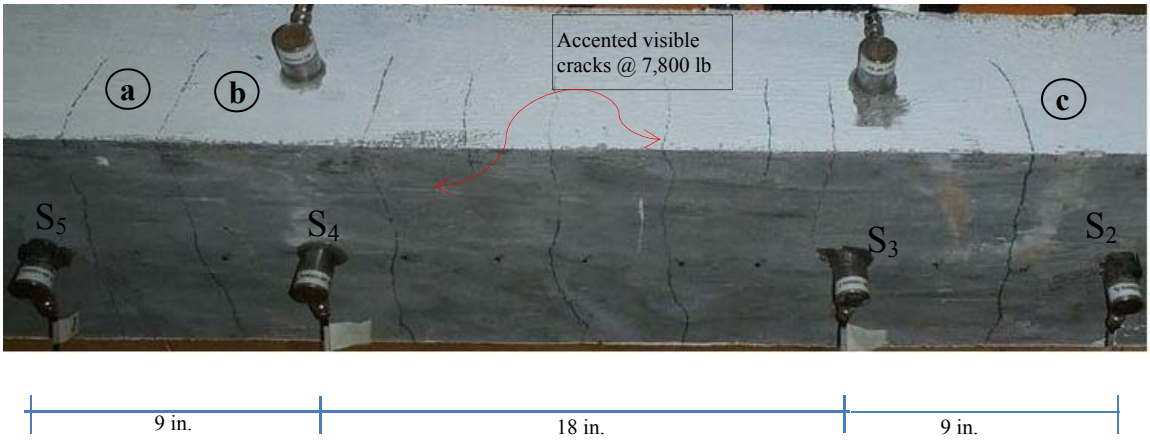

Fig. 4-7. Visible cracks for load step 7 slab S1.

(Note: 1,000 lb=4.448 kN, 1in.=25.4 mm)

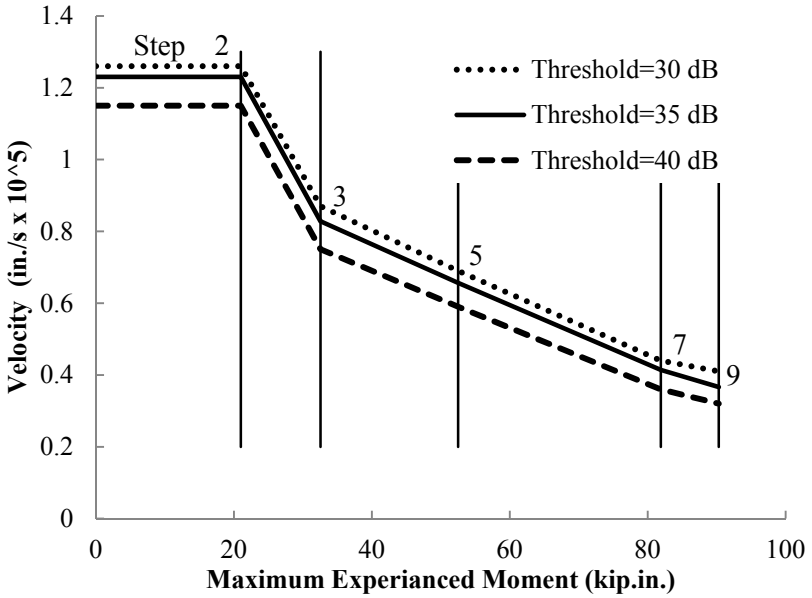

a)

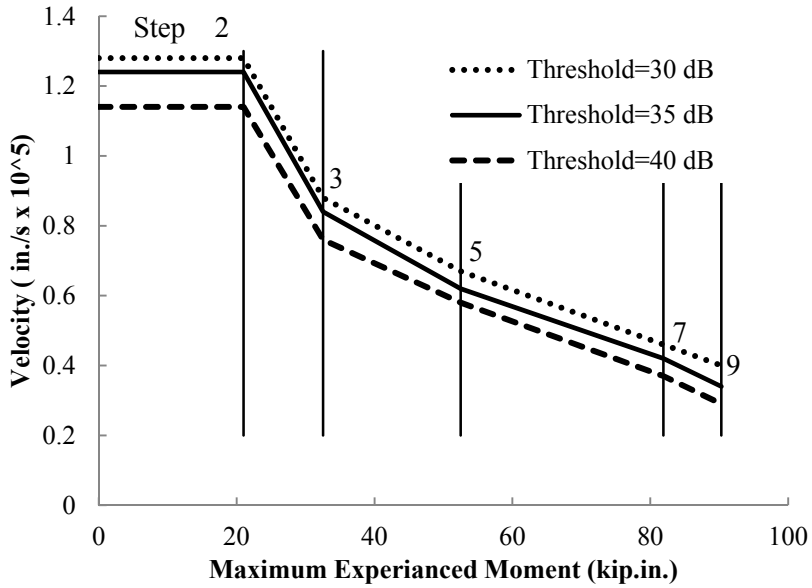

b)

Fig. 4-8. Velocity for different load steps using three threshold levels. : a) Slab S1 b) Slab S2 (Note: 1 lb.in. = 0.113 N.m, 1in. =25.4 mm)

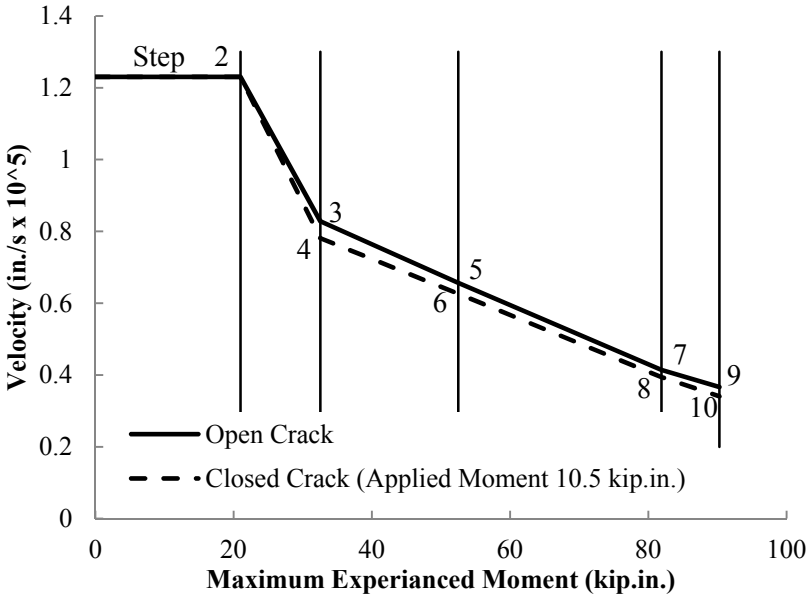

a)

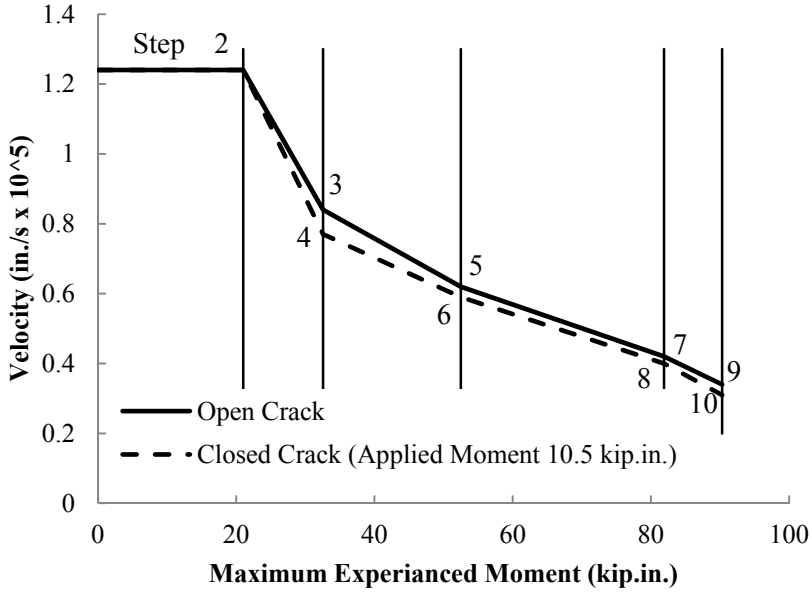

b)

Fig. 4-9. Velocity at different load steps: a) Slab S1 b) Slab S2
(Note: 1 lb.in. = 0.113 N.m, 1 in.=25.4 mm)

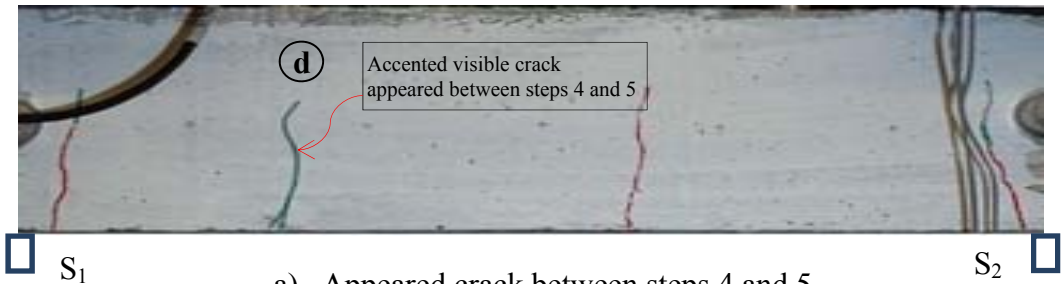

a) Appeared crack between steps 4 and 5

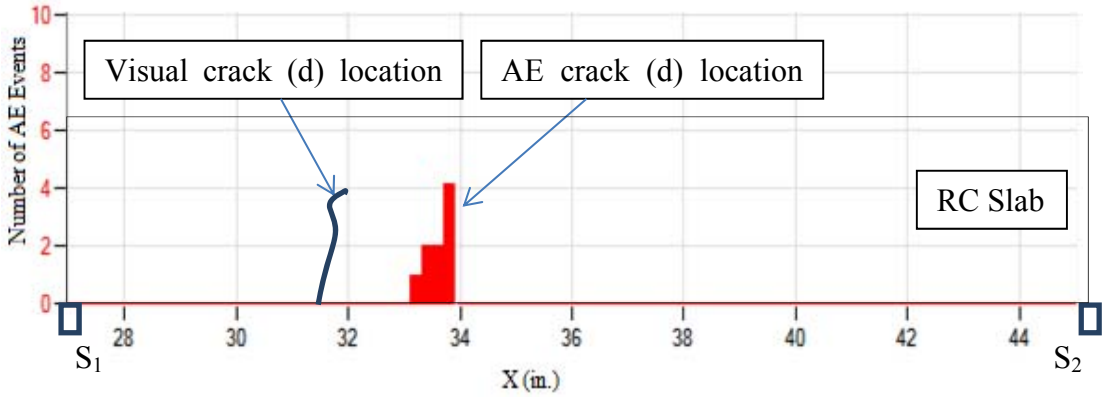

b) New crack vs. AE crack location using un-cracked RC velocity

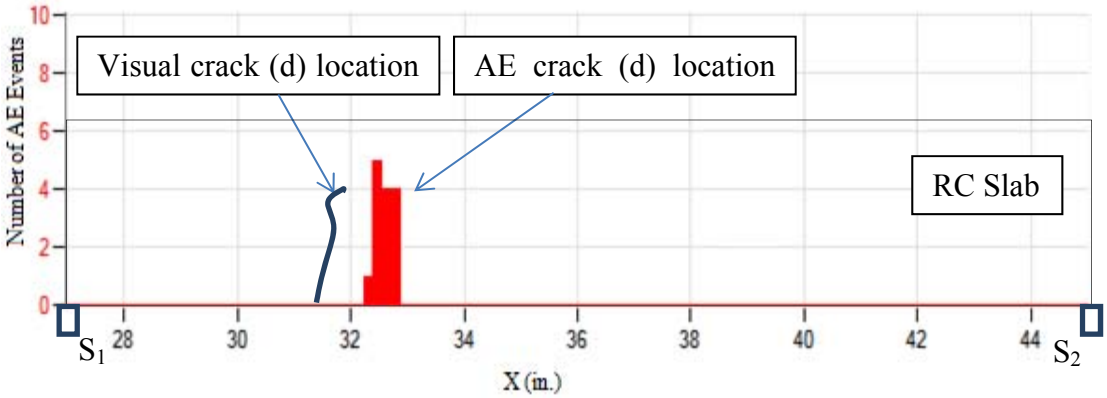

c) New crack vs. AE crack location using cracked RC velocity

Fig. 4-10. New crack and AE crack location overlay (Slab S1)
(Note: 1 in.=25.4 mm)

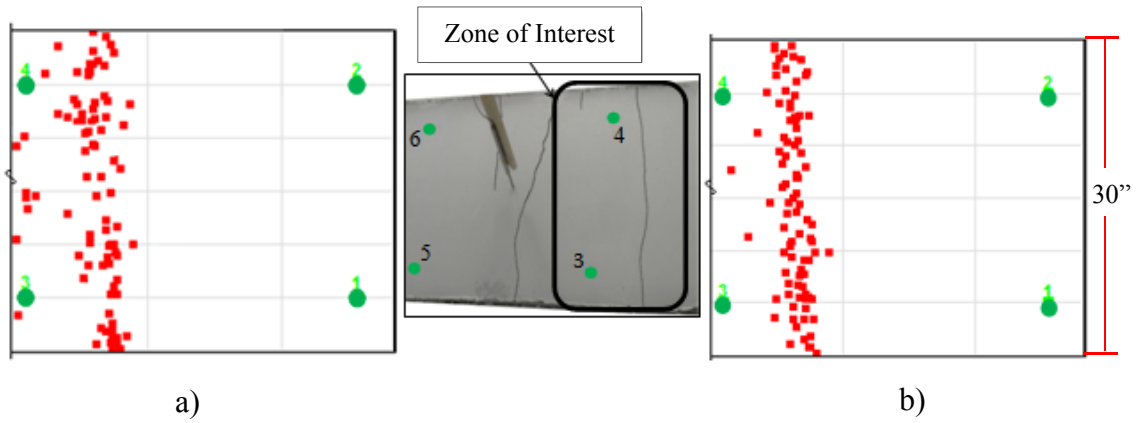

Fig. 4-11. Crack location of study 1 for loads between 5000 to 6000 lb using wave velocity from: a) study 1 b) study 3
(Note: 1,000 lb=4.448 kN, 1in.=25.4 mm)

CHAPTER 5: CONCLUSIONS

This dissertation is articulated in three studies. A novel technique is described based on signal processing and sensor arrangement to process multisensory AE data generated by the onset and propagation of cracks in the first study. The technique is validated with experimental results from an in-situ load test on RC slabs. Approaches for establishing sensor arrangement, TOA selection, velocity optimization and data filtering are introduced. Sequence of controlled crack propagation, in RC strips is observed and it is demonstrated that the AE technique is able to locate the cracks with limited number of sensors (i.e., eight per strip) while they are forming and in some cases before they are visible. The introduced procedure can be used as a component of a structural load testing.

The last two studies cover attenuation and wave velocity in concrete members as these parameters have a prominent effect on applicability of AE and AE source location technique. In the second study a set of AE experiments are conducted on concrete slabs in order to identify the influence of variable parameters including strength, unit weight, aggregate size, aggregate type, geometry, moisture and presence of steel on wave velocity and attenuation. With limited number of tests performed, limited specimen geometries and a typical sensor arrangement, reference tables for wave attenuation and velocity for AE monitoring application in concrete members with abovementioned variable parameters are developed. Obviously, the range of variable parameters can be widely expanded to include various AE sensors, sensor arrangements, geometries, etc. Some observations made for AE wave velocity and attenuation in the specimens are as follow:

- With maturing in concrete, wave velocity increases while attenuation decreases;
- Concrete strength seems not to have an influence on attenuation, but AE signals have a higher velocity through concrete members with higher concrete strength;
- While concrete aggregate size does not affect attenuation, increasing the aggregate size decreases wave velocity;
- Wave velocity for the lightweight concrete is higher than that of normal weight concrete with similar compressive strength;
- Presence of steel reinforcement increases signal attenuation and velocity;
- Attenuation increases with slab thickness while velocity decreases;

Effects of cracks on AE wave propagation in RC media is investigated in the third study. Based on the two test specimens with similar attributes, it is observed that with cracking, velocity decreases and attenuation increases. Crack-to-specimen depth ratio was chosen and used as the parameter describing the severity stage of the cracking in the specimen. Crack to specimen depth ratio shows a direct relationship with the attenuation and an inverse relationship with wave velocity in the media. The results show that closed cracks in unloaded RC member can affect signal attenuation and velocity almost as severely as open cracks under loading. The observations from the last study complements the database for un-cracked concrete slabs introduced in the second study and provides practical information about the wave propagation in cracked RC members especially valuable when source location and filtering are concerned.

The efforts summarized in this dissertation can provide guidance for sensor arrangement, velocity and attenuation assumption for AE monitoring performed on RC slabs and the

outcome can aid the applicability of AE and an AE source location technique in RC members. However, it needs to be noted that the observations are based on limited test specimens and for only one type of resonance AE sensor. Various RC member geometries, aggregates, reinforcement ratios and configuration, sensor positioning configurations need to be tested in a lab environment to produce a more comprehensive database that supports SHM of RC structures in the field.

APPENDIX 1: NOISE FILTERING CONSIDERATION

In all three studies, the recording threshold levels were set higher than the environmental noise. In order to assess the environmental noise amplitude level, a noise test was performed prior to each main test in which the AE equipment recorded the environmental noise for at least ten minutes. Consequently, the test threshold level was set higher than recorded environmental noise amplitude level. In order to eliminate unwanted AE signals coming from loading fixtures or other sources, guard sensor technique was implemented as a post processing procedure. In this step of filtering both AEWin and NOASIS software packages were utilized. The guard sensor technique is a commonly used way of filtering non-relevant signals based on the sequence of arrival times for AE signals at different sensors. As a result, all remaining signals were assumed to be relevant however it cannot be claimed that all non- relevant signals were filtered out or all filtered signals were non-relevant.

The remaining signals then were waveform filtered iteratively as described in the section 2.3.3 of study 1 (column 4 in **Fig. 2-4**). **Fig. A-1** shows the before and after filtering source location results for a line of PLBs performed during the pre-test of study 1 (**Fig. 2-3**). As seen in **Fig. A-1 a**, some events were located far from the PLB line before filtering. **Fig. A-1 b** shows the improvement in location results after using the filtering procedures described above.

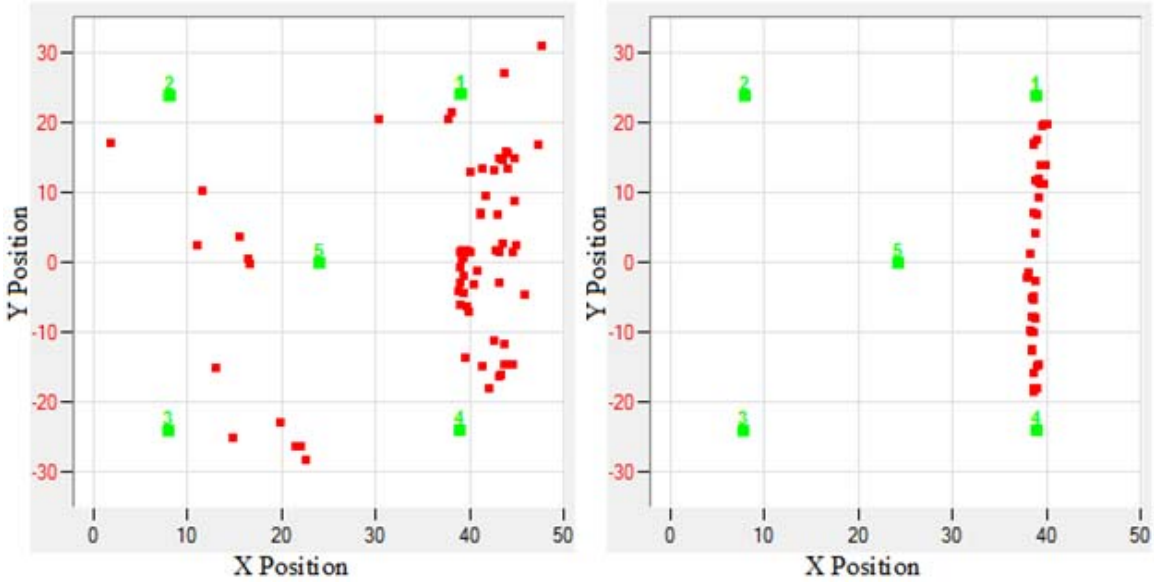

a) b)

Fig. A-1. PLBs location in study 1 before and after filtering

NOTATIONS

D_i: known distance between sensor i and the source

d_i: calculated distance between sensor i and the source

E_D: overall error

E_{XY}: minimum square root of the sum of the squares error

n: number of artificially created sources (PLBs)

R_{es}: radius of efficacy of sensors

t_0: time of event occurrence

t_i: arrival time to sensor i

X_j : exact x coordinate of the PLB j

x_0 : unknown x coordinate of the source

x_{cj} : computed x coordinate of the PLB j

x_i : known x coordinate of sensor i

Y_j : exact y coordinate of the PLB j

y_0 : unknown y coordinate of the source

y_{cj}: computed y coordinate of the PLB j

y_i : known y coordinate of sensor i

z_0: unknown z coordinate of the source

z_i: known z coordinate of sensor i

ΔD_j: difference of exact distances of PLB j to the end sensors

Δd_j: difference of calculated distances of PLB j to the end sensors

Δt_j: difference of arrival time of PLB j to the end sensors

BIBLIOGRAPHY

ACI 437R-03 (2003), *Strength Evaluation of Existing Concrete Buildings*, ACI, Farmington Hills, MI.

AEwin Software User's Manual (2009), Physical Acoustic Corporation, Princeton Junction, NJ.

Al-Wardany, R., Ballivy, G., Gallias, J. L., Saleh, K. and Rhazi, J. (2007), "Assessment of Concrete Slab Quality and Layering by Guided and Surface Wave Testing," *ACI Mater. J.,* 104, 268-275.

ASTM Standard C39 (2010), *Standard Test Method for Compressive Strength of Cylindrical Concrete Specimens*, ASTM International, PA.

ASTM Standard E1316 (2010), *Standard Terminology for Non Destructive Examination*, ASTM International, PA.

ASTM Standard E976 (2010), *Standard Guide for Determining the Reproducibility of Acoustic Emission Sensor Response*, ASTM International, PA.

Baron, J. and Ying, S. (1987), Acoustic Emission Source Location, in: R. Miller, P. McIntire (Eds.), *Nondestructive Testing Handbook Second Edition, Vol. 5: Acoustic Emission Testing, American Society for Nondestructive Testing*, pp. 136–154.

Carpinteri, A., Lacidogna, G. and Manuello, A. (2008), *Localization Accuracy of Microcracks in Damaged Concrete Structures*, *Acoustic Emission and Critical Phenomena*, Taylor & Francis Group, London, 103-124.

Chang, T. P., Lin, H. C., Chang, W. T. and Hsiao, J. F. (2006), "Engineering Properties of Lightweight Aggregate Concrete Assessed by Stress Wave Propagation Methods," *Cement Concrete Comp. J.,* 28, 57-68.

Ding, Y., Reuben, R. L., Steel, J. A (2004), "A New Method for Waveform Analysis for Estimating AE Arrival Times Using Wavelet Decomposition", *NDT & E International,* 37, 279-290.

De Luca, A., Zadeh, J. H. and Nanni, A. (2011), "In-Situ Load Testing: Assessment of the One Way Performance of Reinforced Concrete Slabs," *Accepted for publication by ACI Structural Journal.*

Gassman, S.L. and Tawhed, W.F. (2004), "Nondestructive Assessment of Damage in Concrete Bridge Decks," *J. Perform. Constr. Fac. ASCE,* 220-231.

Gong, Z., Nyborg, E.O. and Oommen, G. (1992), "Acoustic Emission Monitoring of Steel Railroad Bridges," *Materials Evaluation,* 50(7), 883-887.

Gostautas, R.S., Ramirez, G., Peterman R.J. and Meggers, D. (2005), "Acoustic Emission Monitoring and Analysis of Glass Fiber-reinforced Composites Bridge Decks," *J. Bridge. Eng.,* 10(6), 713-721.

Grosse, C.U. and Ohtsu, M. (2008), *Acoustic Emission Testing*, Springer.

Grosse, C. U. and Finck, F. (2006), "Quantitative Evaluation of Fracture Processes in Concrete using Signal-based Acoustic Emission Techniques," *Cement Concrete Comp. J.*, 28, 330–336.

Guratzsch, R. F. and Mahadevan, S. (2010), "Structural Health Monitoring Sensor Placement Optimization under Uncertainty," *American Ins. of Aeronautics and Astronautics J.*, 48(7), 1281-1289.

Han, S. H., Lee, W. J., Cho, H. D. and Kim, D.G. (2001), "Crack Source Location Technique for Plain Concrete Beam Using Acoustic Emission," *J. Korean Concrete Institute*, 13(2), 107-113.

Kim, D. S., Seo, W. S. and Lee, K. M. (2006), "IE-SASW Method for Nondestructive Evaluation of Concrete Structure," *NDT &E International,* 39, 143-154.

McLaskey, G. C. and Glaser, S. D. (2007), "Temporal Evaluation and 3D Location of Acoustic Emission Produced from the Drying Shrinkage of Concrete," *Advances in Acoustic Emission J., 6, 52-57.*

Miller, R. K. and Mclntire, P. (1987), *Non-Destructive Testing Handbook, Vol. 5, Acoustic Emission Testing*, American Society for Nondestructive Testing, USA.

Muhamad Bunnori, M., Pullin, R., Holford, K.M. and Lark, R.J. (2006) "A Practical Investigation into Acoustic Wave Propagation in Concrete Structures," *Adv. Mat. Res. J.,* 13–14, 205–212.

Philippidis, T.P., Anggelis, D. G. (2005), "Experimental study of wave dispersion and attenuation in concrete," *Ultrasonics J.,* 43, 584-595.

Ohtsu, M. and Yuyama, S. (2000), "Recommended Practice for in situ Monitoring of Concrete Structures by Acoustic Emission," *Japanese Society for Nondestructive Inspection*.

Ohtsu, M., Uchida, M., Okamoto, T. and Yuyama, S. (2002) "Damage Assessment of Reinforced Concrete Beams Qualified by Acoustic Emission," *ACI Structural J.,* 99(4), 411-417.

Salinas, V., Vargasa, Y., Ruzzanteb, J. and Gaetea, L. (2010), "Localization Algorithm for Acoustic Emission,". *Physics Procedia*, 3, 863-871.

Shokri, T. and Nanni, A. (2013), "Crack Source Location by Acoustic Emission Monitoring Method in RC Strips during In-Situ Load Test," *Accepted for publication by Smart Struct. Syst.*

Shull, P. J. (2002), *Nondestructive Evaluation Theory, Techniques, and Applications*, Marcel Dekker Inc, New York, NY.

Tobias, A. (1976), "Acoustic Emission Source Location in Two Dimensions by an Array of Three Sensors," *Non-Destructive Testing*, 9(1), 9–12.

Vannoy, D. W., Hariri, R. and Frantzis, C. D. (1991), "Acoustic Emission Investigation and Signal Discrimination in Highway Bridge Applications*," Research report*, Maryland State Highway Administration, FHWA/MD-91/05.

Weiler, B., Xu, S. L. and Mayer, U. (1997), "Acoustic Emission Analysis Applied to Concrete under Different Loading Conditions," *Otto-Graf J.*, 8, 255–272.